University of Dundee

SUMO protease SENP6 protects the nucleus from hyperSUMOylation-induced laminopathy-like alterations

Liczmanska, Magda; Tatham, Michael H.; Mojsa, Barbara; Eugui-Anta, Ania; Rojas-Fernandez, Alejandro; Ibrahim, Adel F.M.

[Link to publication in Discovery Research Portal](#)

SUMO protease SENP6 protects the nucleus from hyperSUMOylation-induced laminopathy-like alterations

Graphical abstract
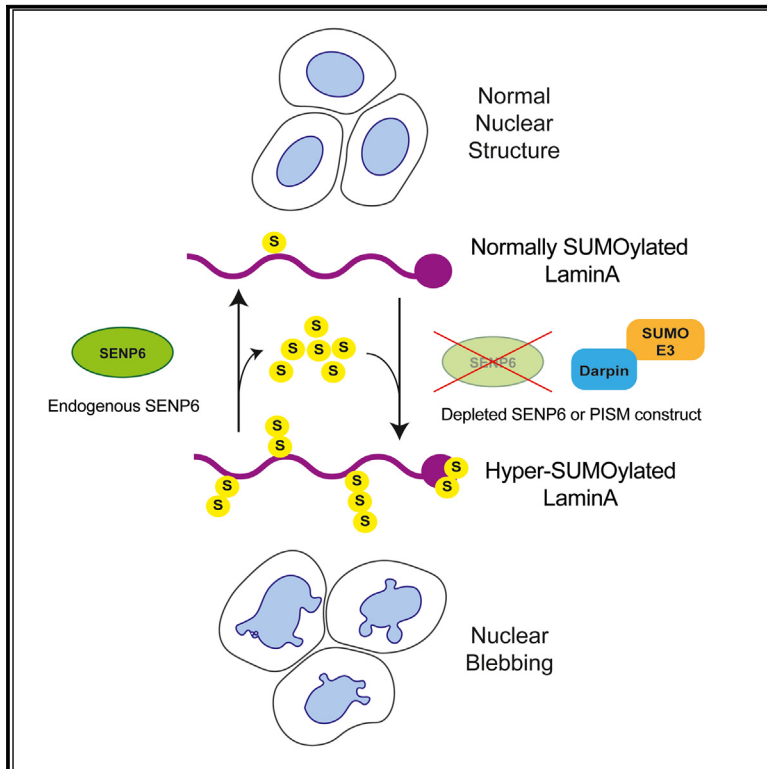
Authors

Magda Liczmanska, Michael H. Tatham,
Barbara Mojsa, Ania Eugui-Anta,
Alejandro Rojas-Fernandez,
Adel F.M. Ibrahim, Ronald T. Hay

Correspondence

r.t.hay@dundee.ac.uk

In brief

The SUMO protease SENP6 preferentially cleaves between SUMO molecules in polySUMO chains. Liczmanska et al. show depletion of SENP6 leads to hyperSUMOylation of lamins A and B and nuclear blebbing reminiscent of laminopathies. Forced hyperSUMOylation of lamins generates the same nuclear phenotype, implying SENP6 functions to suppress adventitious lamin SUMOylation.

Highlights

- The SUMO protease SENP6 regulates lamin protein SUMOylation

- Sites of SUMOylation in lamin A are close to sites of mutations that cause laminopathies

- Depletion of SENP6 leads to laminopathy-type phenotypes in cultured cells

- Specific SUMOylation of lamin A can be induced using a DARPin-SUMO-E3 construct

Article

SUMO protease SENP6 protects the nucleus from hyperSUMOylation-induced laminopathy-like alterations

Magda Liczmanska,[1] Michael H. Tatham,[1] Barbara Mojsa,[1] Ania Eugui-Anta,[1] Alejandro Rojas-Fernandez,[1,2] Adel F.M. Ibrahim,[1] and Ronald T. Hay[1,3,*]

[1]Division of Molecular, Cell and Developmental Biology, School of Life Sciences, University of Dundee, Dow Street, Dundee DD1 5EH, UK
[2]Present address: Instituto de Medicina & Centro Interdisciplinario de Estudios del Sistema Nervioso (CISNe), Universidad Austral de Chile, Valdivia, Chile
[3]Lead contact
*Correspondence: r.t.hay@dundee.ac.uk
https://doi.org/10.1016/j.celrep.2023.112960

SUMMARY

The small ubiquitin-like modifier (SUMO) protease SENP6 disassembles SUMO chains from cellular substrate proteins. We use a proteomic method to identify putative SENP6 substrates based on increased apparent molecular weight after SENP6 depletion. Proteins of the lamin family of intermediate filaments show substantially increased SUMO modification after SENP6 depletion. This is accompanied by nuclear structural changes remarkably like those associated with laminopathies. Two SUMO attachment sites on lamin A/C are close to sites of mutations in Emery-Driefuss and limb girdle muscular dystrophy. To establish a direct link between lamin SUMOylation and the observed phenotype, we developed proximity-induced SUMO modification (PISM), which fuses a lamin A/C targeting DARPin to a SUMO E3 ligase domain. This directly targets lamin A/C for SUMO conjugation and demonstrates that enhanced lamin SUMO modification recapitulates the altered nuclear structure manifest after SENP6 depletion. This shows SENP6 activity protects the nucleus against hyperSUMOylation-induced laminopathy-like alterations.

INTRODUCTION

Post-translational modification with ubiquitin (Ub) and ubiquitin-like proteins (Ubls) is a widely used and versatile strategy to change the biological activity of target proteins in a precise and reversible manner. As Ub and Ubls can form polymers through internal acceptor residues, the information content of complex polymers is potentially extremely high. While all potential Ub-Ub linkages have been detected *in vivo*, only a few chains have been assigned particular biological functions. K11 and K48 linked chains target modified proteins to the proteasome for degradation, and K63 linked chains tend to be non-degradative but rather are involved in signaling processes. Like Ub, the small ubiquitin-like modifier (SUMO) has the potential to form chains.[1,2] In higher eukaryotes, there are three conjugation competent forms of SUMO. While SUMO2 and SUMO3 are virtually identical and collectively termed SUMO2/3, SUMO1 is less than 50% identical to SUMO2/3. The predominant form of SUMO chains is a polymer of SUMO2/3 linked via K11. This lysine residue resides in a consensus SUMO modification site ψKxE, where the amino acid preceding the acceptor lysine is a large hydrophobic residue. Although this is the predominant linkage in SUMO chains, other linkages including sites in SUMO1 have been detected both *in vivo* and *in vitro*.[3–5] SUMO conjugation to substrates and SUMO chain formation are mediated by an enzymatic cascade typical of Ub and Ubls. The first step in the conjugation reaction is carried out by the E1 SUMO-activating enzyme, a heterodimer of SAE1 and SAE2.[6] The E1 uses ATP to adenylate the C terminus of processed SUMO, before removing the AMP and forming a thioester bond between its active site cysteine and the C terminus of SUMO. The SUMO is then transferred from the E1 to form a thioester bond with an active site cysteine in Ubc9, the single E2 SUMO-conjugating enzyme. SUMO-loaded Ubc9 has the ability to directly recognize the ψKxE SUMO consensus modification sequence and transfer SUMO onto the lysine residue in this sequence.[7] However, a small number of SUMO E3 ligases facilitate modification *in vivo*. SUMO chains can be assembled by the same enzymatic machinery, with Ubc9 recognizing the ψKxE motif in SUMO2/3 to catalyze self-assembly. Chains can be assembled with Ubc9 alone, but this reaction is greatly accelerated in the presence of SUMO E3 ligases. The readers of SUMO modification are effector proteins containing SUMO interaction motifs (SIMs), which are short stretches of hydrophobic amino acids usually flanked by acidic residues.[8–11]

Under normal conditions, the SUMO status of substrates is maintained by balancing SUMO conjugation with protease-mediated deconjugation. The dynamic nature of this homeostatic mechanism is evident when conjugation is blocked by inhibitors of the SUMO activating enzyme. In the absence of

conjugation, SUMO-specific proteases rapidly strip SUMO from substrates.[12] In human cells, there are three families of SUMO-specific proteases: the SENPs, which are part of the C48 cysteine protease class[13]; the deSUMOylating peptidases 1 and 2[14]; and USPL1, which is homologous to deubiquitinating enzymes but specific for SUMO.[15,16] The SENPs perform three separate activities in SUMO metabolism. Prior to conjugation, SENPs use their C-terminal hydrolase activity to process SUMO precursors to the mature forms. This requires a highly accurate cleavage after the second glycine residue in the –GG motif to expose the carboxyl group that forms the isopeptide bond with the ε-amino group of lysine in the target protein. To maintain homeostasis, SENPs use their isopeptidase activities to deconjugate SUMO from substrates and to depolymerize substrate-attached SUMO chains. The human SENPs have a conserved protease domain that is homologous to the yeast *Saccharomyces cerevisiae* proteases Ulp1 and Ulp2.[13] Human SENP1, SENP2, SENP3, and SENP5 are related to Ulp1, whereas SENP6 and SENP7 are related to Ulp2.[17] Given the sequence conservation across the protease domains, it is likely that all the SENPs will have a catalytic mechanism similar to that determined for SENP1 and SENP2.[18,19] In human cells, SENP6 and SENP7 appear to be the two SENPs responsible for the depolymerization of SUMO chains. They both preferentially cleave after SUMO2/3 rather than SUMO1, and, while they can remove a single SUMO from a model substrate such as RanGAP1, cleavage between two adjacent SUMO moieties in a chain is more efficient.[20–24] SENP6 depletion in cells results in the accumulation of long SUMO chains and a range of different phenotypes linked to kinetochore assembly,[25] maintenance of centromeric chromatin,[26,27] genome maintenance,[28] and promyelocytic leukemia (PML) body dynamics.[24] Most recently, it has been demonstrated that genetic alteration of SENP6 drives lymphomagenesis and genetic instability in diffuse large B cell lymphoma.[29]

Here, we demonstrate that SENP6 depletion results in hyper-SUMOylation of lamins with accompanying changes to nuclear structure and lamin A/C distribution that are remarkably like those associated with laminopathies: genetic diseases caused by mutations in the genes encoding lamins. Two of the three SUMO attachment sites on lamin A/C are immediately adjacent to sites of mutations in the laminopathies Emery-Driefuss and limb girdle muscular dystrophy. To directly link the laminopathy-like phenotype observed after SENP6 depletion and accumulation of SUMO on lamins, we developed proximity-induced SUMO modification (PISM), in which a lamin A/C targeting DARPin is linked to a SUMO E3 ligase module. This facilitates specific and regulated SUMO modification of endogenous lamin A/C. It was therefore demonstrated that SUMO modification of lamin A/C recapitulates the damage to the nuclear lamina seen after SENP6 depletion and typical of certain laminopathies.

RESULTS

A proteomic strategy for the identification of SENP6 substrates

SUMO modification status is tightly regulated by the opposing activities of the SUMO conjugation machinery and SUMO-spe-

cific proteases. SENP6, like SENP7, appears to prefer SUMO chains over SUMO-substrate linkages.[20,21] While lysines at position 11 in SUMO2 and SUMO3 are thought to be the major branch points of SUMO-SUMO chains, there is evidence that most lysines in SUMO1 and SUMO2/3 are capable of forming conjugates with other SUMO moieties (see www.phosphosite.org). As SENP6 preferentially cleaves SUMO-SUMO linkages, it is predicted that depletion of the protease should lead to increased SUMO-SUMO branching, although the precise topology of the resultant chains is difficult to elucidate. Understanding the biological roles of SENP6 requires the identification of its direct substrates, namely proteins upon which SUMO chains are truncated by SENP6. We therefore developed a proteomic strategy based on the ability of SENP6 to modulate SUMO chain length on target proteins. This SDS-PAGE "slice-by-slice" analysis allows changes to SUMO chain length to be assessed by analyzing differences in the apparent molecular weight (MW_{App}) of SUMO2-modified proteins isolated from cells, which has previously been used to monitor the modification status of SUMO substrates in SDS-PAGE gels.[30,31] After depletion of SENP6, it is expected that its substrates will accumulate longer SUMO chains, resulting in an increase in MW_{App} (Figure 1A). To facilitate this, a novel proteomic approach was developed using SENP6 depletion in HeLa cells expressing close to endogenous levels of SUMO2 N-terminally tagged with 6His to identify SUMO2 target proteins sensitive to the protease. These cells have been used in multiple studies to monitor SUMO substrates with no evidence the tag or the expression levels affect the specificity of conjugation. 6His-SUMO2 HeLa were transfected in triplicate with non-targeting (siNT) or SENP6-targeting (siSENP6) small interfering RNA (siRNA) to deplete levels of protease (Figure 1B) and then SUMO2-conjugated proteins were enriched from cell lysates using nickel nitrilotriacetic acid (NiNTA) affinity chromatography. SUMO-modified proteins were fractionated according to molecular weight (MW) by SDS-PAGE and visualized by Coomassie blue staining (Figure S1A). The gel was cut into 21 slices (Figure S1A) and each gel fragment was subjected to in-gel trypsin digestion. Mass spectrometry (MS) data obtained from each peptide sample delivered protein identity and intensity information for each gel fragment. From these, the distribution of proteins through the gel and the potential change in MW_{App} of thousands of putatively SUMO2-modified proteins after SENP6 knockdown were assessed. By assigning an average MW_{App} to each gel piece (Figures S1B and S1C) and combining this with peptide intensity data from individual proteins, we were able to determine an average MW_{App} for each protein identified (see STAR Methods for details). For example, the estimated average MW_{App} of SUMO2/3 in control samples was 63.3 kDa, whereas, in SENP6-depleted samples, the average MW_{App} was 95.9 kDa, an increase of 32.6 kDa (p = 7.8 × 10^{-6}) (Figure 1C). SUMO2/3 changes the most in the lowermost and uppermost regions of the gel, representing unconjugated and conjugated SUMO2 respectively (Figure 1D, upper panel). Analysis of total SUMO2/3 levels revealed no significant difference after SENP6 depletion (Figure 1D, lower panel). Changes to SUMO2/3 distribution, particularly in the 100- to 250-kDa MW region, and in unconjugated SUMO2/3 were confirmed by western blot analysis using a SUMO2/3-specific antibody (Figure 1E).
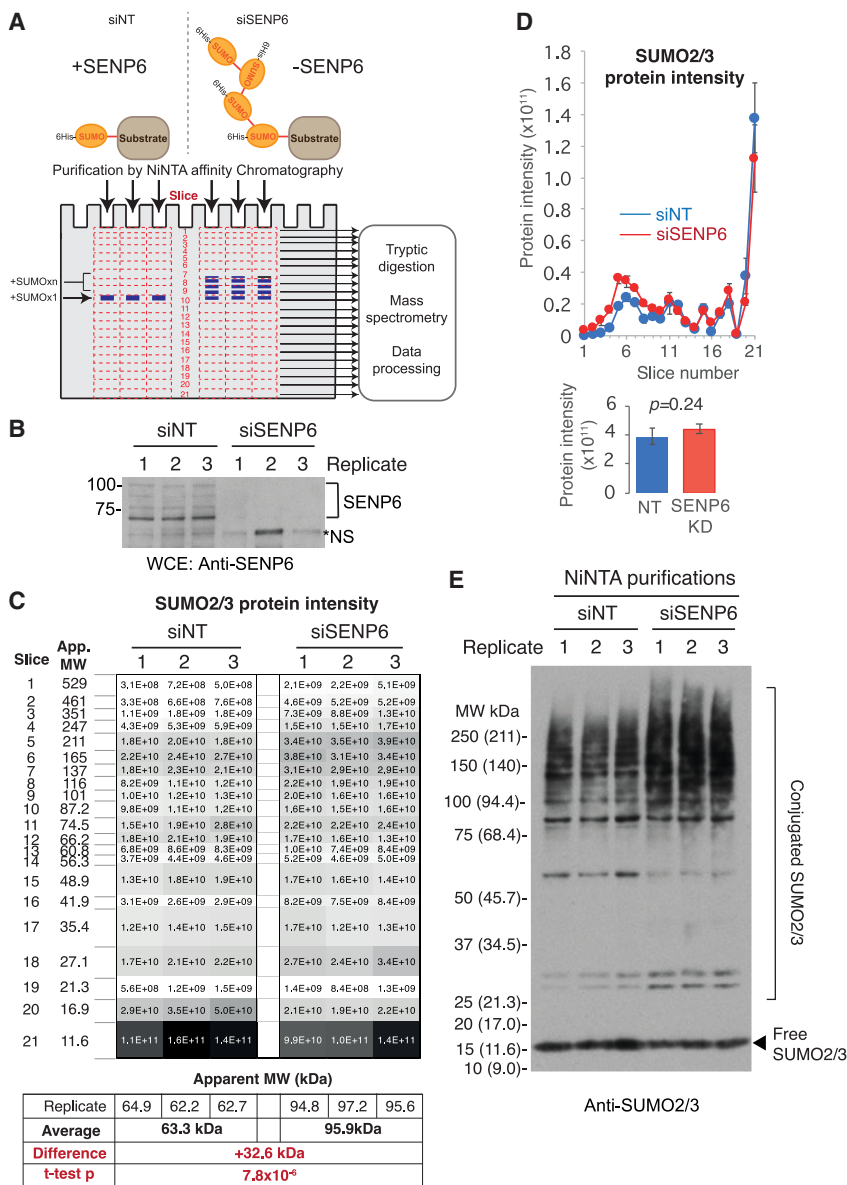
Figure 1. A proteomic approach using electrophoretic mobility change to identify cellular targets of SENP6

(A) Overview of the proteomic method that uses electrophoretic mobility as an indicator of SUMOylation status of proteins purified from 6His-SUMO2 cells.

(B) Anti-SENP6 immunoblot from whole-cell extracts from the samples used for the proteomics experiment to identify SENP6 substrates. *ns, non-specific band.

(C) Visual representation of the MS protein intensity data for the sum of all peptides common to SUMO2 and SUMO3 in each slice across both MS runs. Slices are shaded by intensity. Calculated apparent MW data and Student's two-tailed t test p for the difference in apparent MW between SENP6 and NT siRNA are indicated.

(D) Average protein intensity per slice profile plot (top) and average total protein intensity (bottom) of the data shown in (B) with SD values shown as error bars. p values are calculated by unpaired two-tailed Student's t tests.

(E) SUMO2/3 western blot of NiNTA purifications from 6His-SUMO2 cells after the indicated siRNA treatment. Markers show MW in kDa with apparent MW in this gel system shown in brackets.

lamin A, lamin B1, and lamin B2 all demonstrated a combination of large molecular-weight shifts with significant p values (Figure 2A). The distribution of peptides from SUMO-enriched lamin A/C shows that, from control cells, the average MW_{App} was 67.8 kDa, which increased to 102.3 kDa in material from SENP6-depleted cells (Figure 2B): a difference of 34.7 kDa (p = 5.8 × 10^{-6}) and an increase in overall protein intensity of >2-fold (Figure 2C). This is confirmed by western blot analysis of the NiNTA affinity-purified material from control and SENP6-depleted cells (Figure 2D). Due to the presence of a lamin A/C region with affinity for metal ions (residues 563–566), the unmodified form is enriched in our nickel affinity purifications at 69/62 kDa. The signal is comparable in both conditions, representing similar amounts of unmodified material. In samples from control cells, two species are detected around 100 kDa, which likely correspond to mono-SUMO-modified lamin A and lamin C. In samples from SENP6-depleted cells, these species increase in signal along with forms of higher MW (above 90 kDa), which most likely represent poly-SUMO-modified lamin A/C (Figure 2D). The validity of the slice-by-slice method is supported by the excellent concordance of the virtual western blots (Figure 2B) based on the MS analysis and the conventional western blot data (Figure 2D).

In response to SENP6 depletion, the SUMO-associated forms of lamin B1 and lamin B2 both increased in abundance and displayed MW_{App} increases of 49.5 and 57.5 kDa (p = 2.23 × 10^{-5}

Lamin SUMOylation increases with SENP6 depletion

An increase in the calculated MW_{App} of SUMO-modified species (Figure 1) shows that the slice-by-slice MS analysis has the potential to detect specific SENP6 substrates by virtue of their increase in MW_{App} in response to SENP6 depletion. We calculated the MW_{App} of every protein identified in all replicates in control and SENP6-depleted conditions. The SENP6-dependent shift in MW of each SUMO substrate was then calculated by subtracting the control from SENP6-depleted MWs (see Data S1). To visualize these data, the MW difference of each protein was plotted against the statistical significance of the difference (p value) (Figure 2A). Several recently identified SENP6 substrates, including HNRNPA2/B1, ARHGEF4, ARHGAP21, and centromere protein (CENPC), were identified, but the most conspicuous outliers in this analysis were the lamin family of proteins:
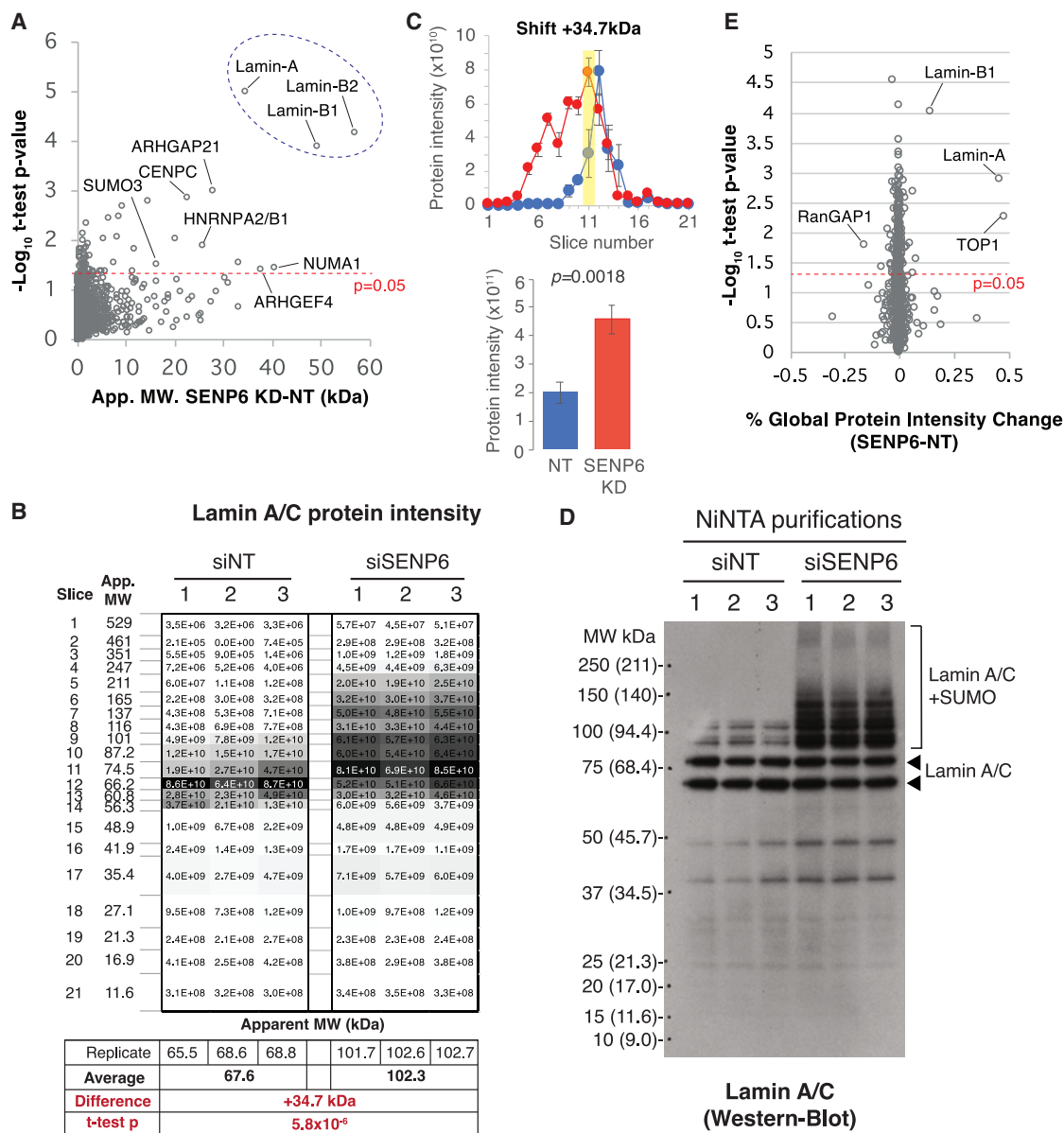
Figure 2. Lamins reduce in electrophoretic mobility and accumulate a large proportion of cellular SUMO2 upon SENP6 depletion

(A) Chart showing SENP6 knockdown-induced MW_{App} shift and statistical significance for proteins detected in nickel affinity purifications from 6His-SUMO2 cells. Points represent the average of the values calculated across the two MS runs. Selected proteins are indicated.

(B) Visual representation of the MS intensity data for lamin A/C for the three replicates of each siRNA treatment by summation of the intensity values from both MS runs.

(C) Profile plot (upper) and total protein intensity data (lower) of the average values of the data shown in (B) with SD values shown as error bars. p value is calculated by unpaired, two-tailed Student's t test.

(D) Lamin A/C western blot of NiNTA purifications from 6His-SUMO2 cells after the indicated siRNA treatment. Markers show MW in kDa with apparent MW in this gel system shown in brackets.

(E) Chart showing relationship between % global protein intensity change and statistical significance of that difference (see STAR Methods for details). Points represent the average of the values calculated across the two MS runs.

and 2.15×10^{-5}), respectively (Figures S2A and S2B). By comparison, CENP-C, previously identified as a SENP6 substrate,[26] displayed an increase in MW_{App} of 22.8 kDa and a 4-fold increase in abundance (Figure S2C). Western blot analysis of the SUMO-associated material confirmed the increases in both abundance and MW_{App} of lamin B1 in response to SENP6 depletion (Figure S2D).

Upon SENP6 depletion, there was an approximately 2-fold change in lamin A abundance in 6His-SUMO2 preps and a ~35-kDa shift in MW_{App}. However, because peptide intensity

ratios and MW shifts only show relative abundance changes, they do not indicate the scale of SUMOylation change with respect to all other substrates. To identify the major acceptors (and donors) of SUMO during SENP6 knockdown, the proportion of the total protein intensity that each protein represented in the MS data was calculated, and the difference between this value for siSENP6 and siNT conditions was determined (see STAR Methods for details). This we define as "% global protein intensity change" and interpret a protein with a large positive or large negative value as representing a major acceptor or donor (respectively) of SUMO under SENP6 depletion. Most proteins showed changes of less than 0.05% of global protein intensity (Figure 2E), indicating their SUMOylation change represented only a small proportion of the total SUMO shifting between proteins. However, TOP1, lamin A, and lamin B1 all showed a significant increase, representing a far greater proportion of the total protein intensity detected in the samples. RanGAP1 was the only protein with a significant decrease in % global protein intensity on a similar scale to the gains shown by lamins and TOP1. The reason for this loss of SUMO under SENP6 knockdown is unclear. Previous work has shown treatments that trigger increases in net SUMOylation usually occur with a concomitant loss of SUMO from a subset of substrates,[4,30] although the precise mechanisms have not been determined. Whether in this instance this is explained by localized SUMO depletion or longer-term indirect changes is unclear. What is clear is these data suggest that not only do lamins experience a large MW shift but they are also among the major acceptors of SUMO molecules during SENP6 depletion.

SUMO-SUMO polymers increase in abundance upon SENP6 depletion

Although SENP6 depletion does not alter total cellular levels of SUMO2 or 3, it does alter their distribution within the gel, increasing higher-MW material and decreasing the free species (Figures 1C–1E). Any SUMO1 and SUMO3 co-purified with 6His-SUMO2 is likely to come from substrates either multiply modified by different SUMO paralogues or from mixed SUMO polymers attached to substrates. Both SUMO1 and SUMO3 paralogues were significantly enriched in our 6His-SUMO2 pulldowns from cells treated with SENP6 siRNA (Figures S3A and S3B). If this is at least partly caused by an increase in SUMO chain length after SENP6 knockdown, this should be manifest by an increase in abundance of SUMO-SUMO linkages that arise from the isopeptide bond formed between the C terminus of one SUMO and a lysine acceptor residue in a linked SUMO. Several types of SUMO-SUMO linkage-specific peptides derived from a variety of SUMO1, SUMO2, and SUMO3 combinations were detected in our MS analysis (Figures 3A–3D; S4A–S4D), all of which increase in abundance after SENP6 depletion. This was particularly evident in the higher-MW region of the gel above 150 kDa (Figures 3A–3D, left charts). These results are indicative of the growth of SUMO chains on substrates in the absence of SENP6 and strongly support the hypothesis that SENP6 is responsible for cleaving SUMO-SUMO bonds *in vivo*.

Substrates linked to SUMO chains can be ubiquitinated by the action of SUMO targeted ubiquitin ligases (STUbLs) resulting in ubiquitin-mediated proteasomal degradation.[32] Notably, the to-

tal peptide intensity for ubiquitin in 6His-SUMO2-enriched fractions was not affected by SENP6 depletion (Figure S5A), nor were peptides indicative of Ub-Ub linkages through lysines 11 and 63 (Figures S5B and S5D). Only K48 chains displayed a change in peptide intensity in response to SENP6 depletion (Figure S5C), although, contrary to the SUMO-SUMO peptides, they were modestly reduced in abundance. This suggests that altered ubiquitination is unlikely to contribute significantly to the increases in MW of SUMO targets during SENP6 depletion.

SENP6 depletion results in increased SUMO modification at sites in lamin A/C adjacent to laminopathy-causing mutations

Formation of the nuclear lamina is an important determinant of nuclear structure that influences chromatin organization and gene expression. Mutations in lamin A/C disrupt formation of the nuclear lamina and are responsible for several genetic diseases collectively termed laminopathies.[33,34] As SUMO modification of lamins at critical sites has the potential to disrupt homotypic interactions required for the assembly of the nuclear lamina, it was important to determine if SUMOylation at specific sites in lamins changes in response to SENP6 depletion. In an attempt to find sites of modification in the data, the MS files were researched in MaxQuant, including variable modifications for the tryptic adducts of SUMO1 and SUMO2/3 (see STAR Methods). While this is not an efficient method for site-level SUMO proteomics, it will identify a small number SUMO-substrate branched peptides from the most abundant conjugates. From this branched peptide search of the MS data, a total of only 23 SUMO modification sites were identified (Data S2). Due to the complexity of tryptic branched peptide tandem MS (MS/MS) spectra, these are difficult to detect in complex peptide samples, and so it is reasonable to suggest that any branched peptides found are likely to be derived from highly modified SUMO substrates. Indeed, along with the SUMO-SUMO peptides already described above, SUMO2 branched peptides from RanGAP1, Ubc9 (UBE2I), and histone proteins were identified along with several sites from lamin proteins. Hierarchical clustering based on normalized peptide intensities showed that the 23 site identifications clustered into two broad groups (Figure 3E), with SUMO-SUMO branched peptides and SUMO-lamin peptides clustering in one group separate from the other branched peptides. This separation is broadly based on a strong increase in abundance with SENP6 knockdown for SUMO-SUMO and SUMO-lamin peptides, and a modest reduction in abundance for the others, such as SUMO2 conjugation at K779 from TRIM28 (Figure 3F). In lamin A, the detected sites were K233, K378, and K420 (Figures 3G–3I and S6A–S6C). Analysis of the intensity distribution of these peptides from each slice of the SDS-PAGE gel revealed that, in the presence of SENP6, these peptides were either undetectable (K233, K378) or present at a relatively low level (K420), and, when SENP6 was depleted, they all increased and appeared in higher-MW regions of the gel (Figures 3G–3I). Remarkably, by comparison with genetic data relating to laminopathies, we found two out of three SUMO modification sites are immediately adjacent to mutations causing Emery-Dreifuss muscular dystrophy 2 (EDMD2): disease mutation G232F is adjacent to SUMO modification site K233, and
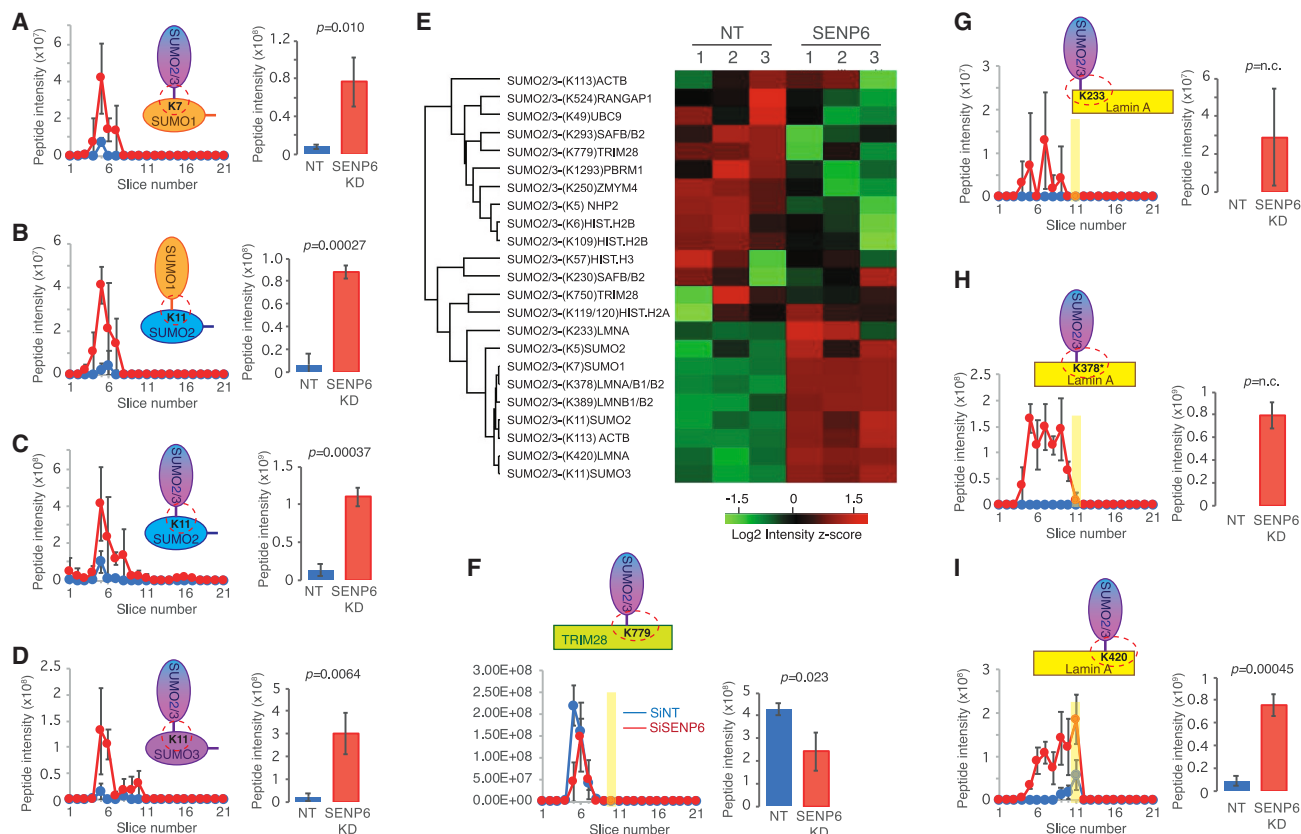
Figure 3. SUMO-SUMO and SUMO-lamin branched peptides are increased in abundance upon SENP6 depletion

(A–D) Slice-by-slice peptide intensity data (left) and total intensity data (right) for the SUMO-SUMO branched peptides indicated. Points represent the average of the triplicate intensity data summed across the two MS runs. SD values shown as error bars and unpaired, two-tailed Student's t test p is indicated for the total intensity data.

(E) Hierarchical clustering of z scores of $\log_2$ intensity values for 23 SUMO-substrate branched peptides detected in 6His-SUMO2 purifications. Zero values were replaced in Perseus to facilitate graphing.

(F) Peptide intensity profile plot and total peptide intensity data for the branched peptide indicative of SUMO2/3-TRIM28 linkage via K779. Yellow region shows the gel slice the unmodified protein would be expected to resolve to.

(G–I) As in (A)–(D) and (F) but for SUMO2/3-lamin branched peptides depicted in the schematics. *Modified peptide for K378 in lamin A is identical to lamin B1 modification at K379. n.c., noncalculable due to zero intensity in siNT samples.

disease mutations R377H and R377L are adjacent to SUMO modification site K378 (Figure 4). The mutation L380S causing muscular dystrophy congenital *LMNA*-related (MDCL) is also close to this site. Both SUMO sites and mutations are in regions known to be involved in lamina assembly. To visualize the location of these sites and how they might influence the formation of higher-order structures, a lamin A dimer was modeled using AlphaFold (Figure S7A). In this model, K233 residues from both chains are in close proximity (Figures S7B and S7C) and are found within a confidently modeled coiled-coil domain. Both K378 residues are also found in close proximity, but the secondary structure is less confidently predicted (Figure S7B). Both K420 residues are in regions predicted to be unstructured and are spatially separated. This suggests that K233 and possibly K378 SUMO modification may disrupt the coiled-coil structure of the dimer and therefore interfere with assembly of the nuclear lamina, as could mutations to these residues or other nearby amino acids.

The phenotype of SENP6 depletion in HeLa cells is reminiscent of cells with laminopathy

As SUMO modification of lamins has the potential to disrupt lamin assembly, we investigated the effect of SENP6 depletion on the integrity of nuclear lamina by immunofluorescence microscopy on HeLa cells using an antibody to lamin A/C (Figures 4B and 4C). Cells were transfected with non-targeting siRNA or an siRNA to SENP6, and, after 72 h, cells were fixed and stained with an antibody to lamin A/C. Cells treated with the non-targeting siRNA revealed the expected pattern of lamin A/C staining in a ring around the nuclear periphery. Nuclei displayed an even, oval shape with few distortions in nuclear structure (Figure 4C). However, a substantial proportion of cells treated with siRNA against SENP6 displayed severely malformed nuclei with extensive blebbing of the nuclear envelope showing extruded regions of the nuclei appearing to have a reduced DNA content, as judged by DAPI staining (Figures 4C and 4D). This phenotype of misshaped nuclei and nuclear blebbing is typical of many laminopathies.
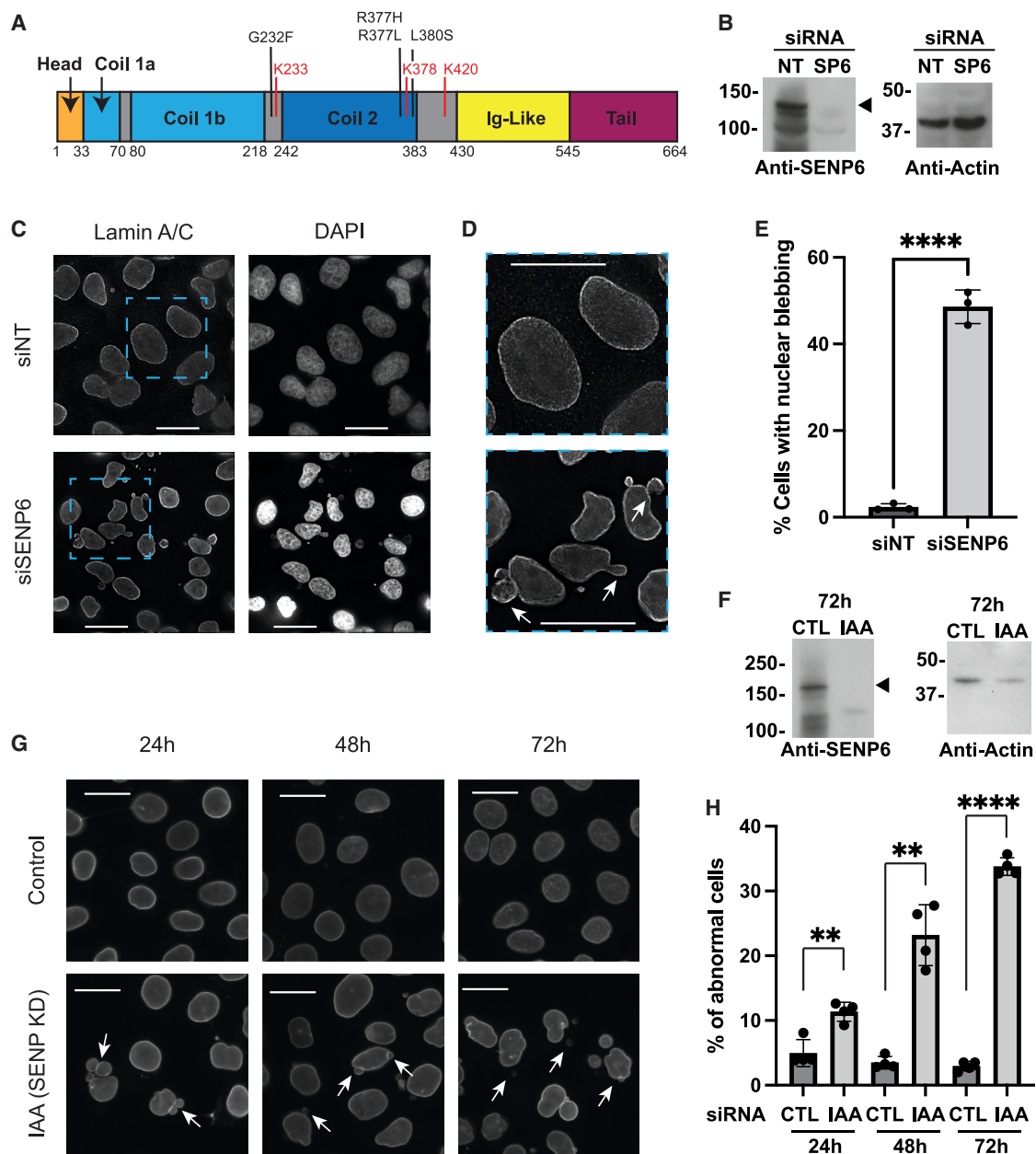
Figure 4. SENP6 knockdown results in abnormal nuclear phenotype

(A) Schematic diagram of lamin A showing the main domains and the positions of SUMOylated lysines (red) relative to proximal laminopathy mutations (black).

(B) Anti-SENP6 and anti-actin western blots from crude extracts from cells used in (C)–(E). SENP6 is indicated with an arrowhead.

(C) Immunofluorescence analysis of HeLa cells treated with either a non-targeting siRNA control or siRNA targeting SENP6 for 72 h and visualized using lamin A/C antibody.

(D) Magnified images of cells from (C) (blue squares). Arrows indicate nuclear blebbing.

(E) Graph showing percentage of HeLa cells exhibiting nuclear blebbing 72 h after transfection with siRNA. Columns show averages and SD of cell counts from triplicate experiments. Results of one-way ANOVA are shown above.

(F) Anti-SENP6 and anti-actin western blots from crude extracts from cells used in (G) and (H). GFP-AID-SENP6 is marked with an arrowhead.

(G) Immunofluorescence analysis of GFP-AID-SENP6-expressing HeLa cells treated with either ethanol (control) or indole-3-acetic acid (IAA) for 24, 48, and 72 h and visualized using lamin A/C antibody.

(H) Graph showing percentage of GFP-AID-SENP6-expressing HeLa cells exhibiting nuclear blebbing after SENP6 knockdown. Columns show averages and SD of cell counts from quadruplicate experiments. Unpaired, two-tailed Student's t test summaries are shown above pairwise comparisons.

Statistical analysis based on cell counting from triplicate transfections revealed about 50% of SENP6 siRNA-treated cells exhibited malformed nuclei, yet less than 5% of cells in control samples displayed the same phenotype (Figure 4E).

Although the specificity of the SENP6 siRNA has been studied previously,[24,35] there remains the possibility that prolonged exposure to SENP6 siRNA could have indirect effects that may explain the observed phenotype. To overcome these issues, we employed a previously described GFP-AID-SENP6 HeLa cell line[27] where rapid degradation of SENP6 could be induced via an auxin-inducible degron by IAA (indole-3-acetic acid) treatment. SENP6 depletion was initiated by the addition of IAA to the medium (Figure 4F) and cells were imaged at 24, 48, and 72 h after SENP6 depletion (Figure 4G). Control samples contained nuclei mainly with the usual oval shape and typical lamin A/C staining of the nuclear envelope that did not change over time. However, in SENP6-depleted cells, the blebbing phenotype was evident after 24 h and continued to increase up to 72 h (Figures 4G and 4H), which may be influenced by multiple passages through the cell cycle.

PISM enables targeting of SUMO to lamins in cells

SENP6 may influence the SUMOylation status of many proteins. Hence, knockdown is potentially pleiotropic. Attributing the observed nuclear malformation phenotype directly to altered lamin SUMOylation is difficult from these experiments alone. Furthermore, mutation of lamin proteins intending to ablate site-specific SUMOylation not only is difficult due to the large number of SUMO acceptor lysines identified (so far totaling 14; phosphosite.org) but also has the potential to directly alter lamin structure, thus making it difficult to associate functional changes directly to SUMO. We therefore developed a method to target a specific cellular protein substrate for SUMO modification and call this PISM. PISM is similar in concept to antibody really interesting new gene (RING)-mediated degradation,[36] where a protein-binding nanobody is fused to a RING domain to mediate ubiquitination of the nanobody bound target. For this application of PISM, a protein targeting designer ankyrin repeat protein (DARPin)[37] fused to a SUMO E3 ligase domain from RanBP2 to drive SUMO modification of the selected target. To achieve this, a lamin A targeting DARPin, previously shown to bind lamin A without disrupting lamin assembly,[38] was fused to the IR1-M-IR2 domain from RanBP2[39–42] (Figure 5A). This particular ligase fragment was chosen as it is relatively short (129 amino acids) and has the capacity to synthesize polymeric, branched SUMO conjugates.[3] When expressed in cells, the PISM construct is directed to the nucleus (due to an encoded nuclear localization signal) where the DARPin sequence binds to lamin A and the RanBP2 SUMO E3 module drives SUMO modification of proximal lysine residues. The efficiency of the lamin A targeting PISM was assessed on HeLa and U2OS cells after transfection of an mRNA encoding the PISM construct. Expression of the myc-tagged PISM protein after 20 h was determined by western blotting (Figure 5B). During expression of the PISM construct, the total levels of lamin A/C appeared unchanged (Figure 5B, short exposure), although there was an increase in higher-MW forms of lamin A/C, consistent with SUMO modification (Figure 5B, long exposure). To provide more controlled expression of the

PISM protein, we generated HeLa cells with doxycycline (DOX)-inducible expression of the PISM construct containing either the lamin A targeting DARPin or a non-targeting DARPin mutant. Immunofluorescence analysis indicated that, while doxycycline-induced expression of the non-targeting PISM construct did not alter lamin A/C staining or nuclear structure, expression of the lamin A/C targeting PISM was accompanied by the appearance of abnormal lamin A/C staining and deformed, blebbed nuclei (Figure 5C) that were similar to those observed after SENP6 depletion (Figure 4). To rule out any SUMO independent effects that might be a consequence of direct binding of the lamin A/C targeting PISM, DOX treatment was also carried out in the presence of the SUMO E1 inhibitor ML792.[12] In this case, expression of the lamin A/C targeting PISM did not alter nuclear structure or lamin A/C staining (Figure 5C), indicating that the observed effects were dependent on SUMO modification.

Targeted SUMO modification of lamins causes a laminopathy-like nuclear phenotype

The abnormal lamin A/C staining and deformed nuclei observed after expression of the PISM construct mimicked SENP6 depletion and were blocked by pharmacological inhibition of the SUMO conjugation pathway. To provide an alternative, genetic means of inhibiting PISM-mediated SUMO modification, mutations predicted to inactivate SUMO E3 ligase activity were introduced into the RanBP2 IR1-M-IR2 module of the PISM construct. However, due to the independent E3 functions of the IR1 and IR2 domains,[39,42,43] it was not possible to accomplish this in the original PISM construct. A second construct was therefore developed in which the IR2 domain of the SUMO E3 ligase module was removed. This allowed mutations to be introduced into the IR1 domain that reduced but did not eliminate SUMO E3 ligase activity. Stable HeLa cell lines were generated in which expression of PISMs was induced with doxycycline and, after 24 h, nuclear lamina was visualized by immunofluorescence with antibody against lamin A/C (Figure 6A). Parental cells without the PISM transgene exhibited regular lamina staining and oval nuclei even the presence of doxycycline. This was also the case in cells with an integrated transgene but in the absence of doxycycline, where PISM expression was repressed. However, when doxycycline was present and cells expressed the high-activity PISM, severe nuclear malformation and delocalization of lamin A/C staining from periphery to the nucleoplasm was evident (Figure 6A). This phenotype mimicked SENP6 depletion and was very similar to certain laminopathies. In the presence of doxycycline expression of the low-activity PISM construct, some abnormal cells were detected, but the phenotype was less severe (Figure 6A). This was statistically confirmed by cell counting from quadruplicate experiments (Figure 6B). Cells containing the high SUMO E3 ligase activity PISM under conditions where expression was repressed displayed low levels of abnormal nuclei (20%–25%), but this rose to over 50% when expression was induced with doxycycline (Figure 6B). Cells containing the low SUMO E3 ligase activity PISM under conditions where expression was repressed also displayed low levels of abnormal nuclei (20%–25%), and, while the percentage of cells displaying abnormal nuclei rose after doxycycline induction of
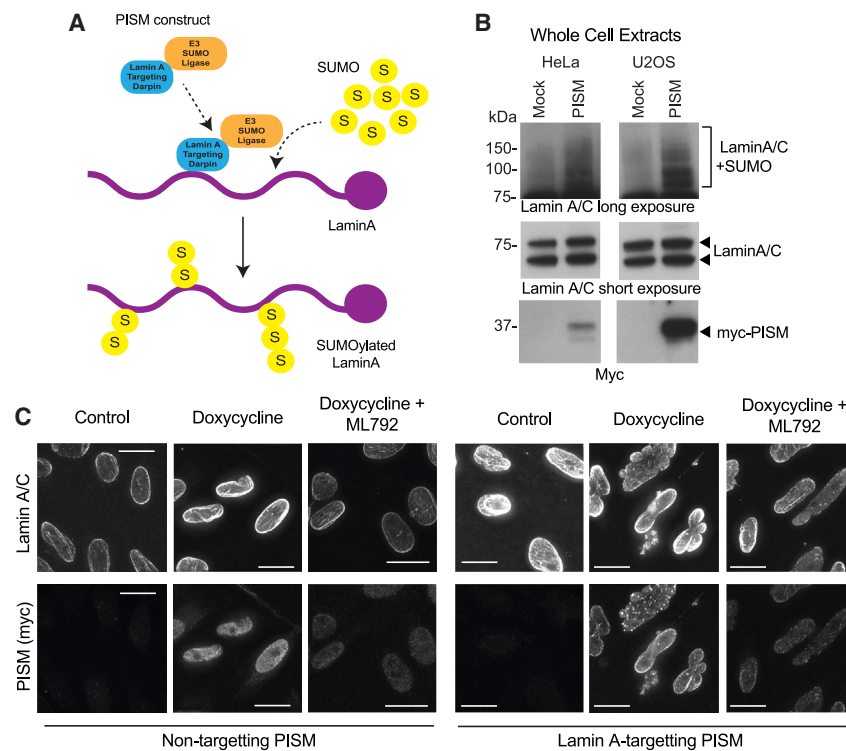
Figure 5. PISM allows targeted SUMOylation of lamin A in cells

(A) Schematic representation of PISM mode of action resulting in SUMO modification of lamin A.

(B) Western blot analysis of crude extracts from HeLa and U2OS cells transfected with myc-tagged lamin A targeting PISM (IR1-M-IR2 E3 module) using antibodies against lamin A/C and Myc.

(C) DOX induction in HeLa Flp-In T-Rex cells of PISM constructs containing either a mutant (non-targeting) DARPin, or the wild-type (WT) DARPin directing the SUMO ligase to lamin A. Dependence on SUMOylation was investigated by co-treatment with ML792. Immunofluorescence images were acquired using anti-lamin A/C and myc antibodies.

PISM expression (40%), this was lower than for the high-activity construct (Figure 6B). Western blot analysis of these samples indicated that both high- and low-activity PISM constructs were expressed at the same level after doxycycline induction, but the extent to which lamin A/C is SUMO modified is greater in the high-activity constructs (Figure 6C, long exposure). Expression of the PISM constructs did not change the cellular levels of lamin A/C (Figure 6C, short exposure). Furthermore, a survey of SUMO substrates that are either well established or known to exist in close proximity to lamin A/C in the cell revealed only the closely associated lamin B1 showed evidence of increased SUMO conjugation during PISM expression (Figures S8A and S8B). Thus, the phenotype of abnormally shaped nuclei with disrupted lamin A/C staining appears to be related to the extent of lamin A/C and perhaps lamin B1 SUMO modification induced by the PISM construct.

It has been previously shown that SUMO chains recruit the STUbL RNF4, which targets polySUMOylated proteins for degradation via the 26S proteasome.[32,44] RNF4 has been shown to become auto-ubiquitinated and degraded in response to SENP6 depletion due to the accumulation of poly-SUMO chains, which activate the ligase.[35] This raises the possibility that the loss of RNF4 during SENP6 knockdown contributes to the blebbing phenotype observed. siRNA depletion of RNF4 in U2OS cells did not trigger the same phenotype seen with SENP6 knockdown, nor did it increase the effect of SENP6 depletion (Figure S9A and S9B). Furthermore, in Flp-In T-REx HeLa cells expressing the PISM construct, which induces the blebbing phenotype, RNF4 levels did not significantly change (Figure S8B). This suggests degradation of RNF4 is not

responsible for the observed phenotype of lamin hyperSUMOylation.

Expression of lamin A targeting PISM in human induced pluripotent stem cells leads to dispersal of lamin A from the nuclear periphery

Although much of our understanding of nuclear structure is based on studies using transformed cells, it appeared that the laminopathy-like phenotype observed after AID-mediated SENP6 degradation (Figure 4E) was related to cells traversing the cell cycle. As many transformed cells have defective cell-cycle checkpoints, it was important to investigate the SENP6 effects upon nuclear lamina in cells with competent cell cycle checkpoints. To this end, lamin A/C targeting PISM constructs with either high or low SUMO E3 ligase activity were introduced into human induced pluripotent stem (hIPS) cells by RNA transfection. After 24 h, cells were stained with antibodies to lamin A/C and analyzed by fluorescence microscopy. Mock-transfected cells exhibited regular lamin A staining at the nuclear periphery and with oval nuclei (Figure 7A). However, expression of PISM constructs in these cells appears to lead to a reduction in the lamin A/C signal, which can be explained by redistribution from its concentrated localization at the nuclear periphery to diffuse staining over the entire nucleus (Figure 7A). Cell counting from quadruplicates showed control cells displayed minimal levels (<5%) of diffused lamin A/C, while expression of the high-activity PISM leads to more than 60% of cells displaying delocalized lamin A/C. This is reduced to about 30% of cells displaying delocalized lamin A/C after expression of the low-activity PISM (Figure 7B). Western blot analysis confirmed that the high- and low-activity PISM constructs were expressed to the same level and that total lamin A/C levels did not change after PISM expression. Higher-MW forms of lamin A/C, consistent with SUMO modification, were apparent after expression of the high-activity PISM but not in cells expressing the low-activity PISM or in mock-transfected cells (Figure 7B). It appears to be the case that hyperSUMOylation of lamins in IPS cells results in redistribution of lamin A/C rather than a nuclear blebbing phenotype, and we speculate that such extreme morphological
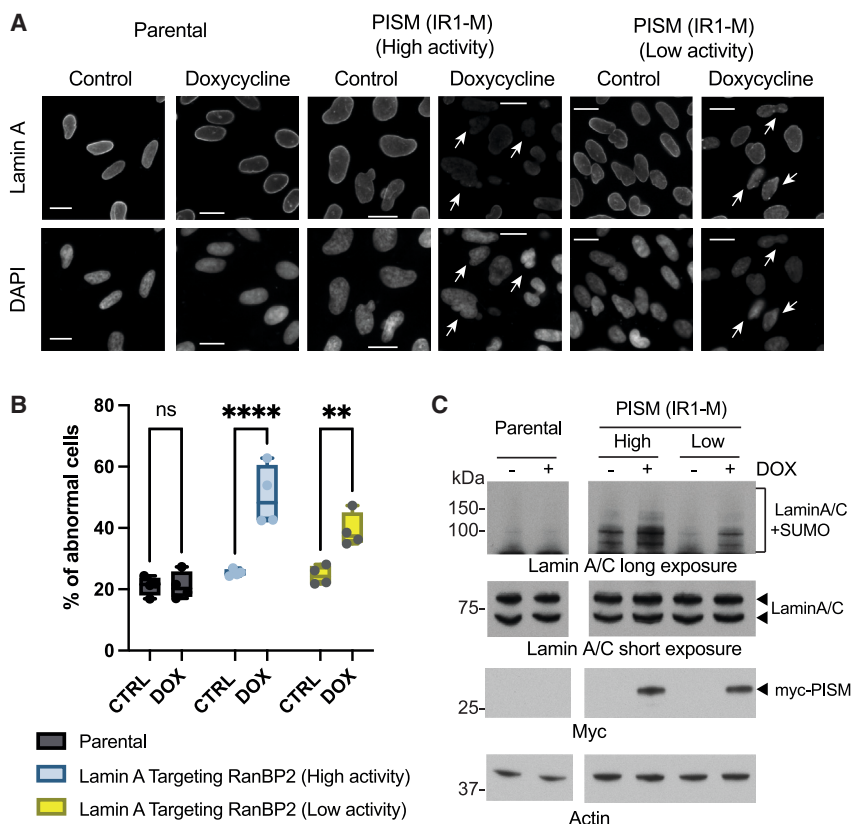
A

B

C

Figure 6. Targeted SUMOylation of lamin A causes laminopathy-like nuclear phenotype

(A) Parental and myc-tagged lamin A targeting PISM (IR1-M high- and low-activity forms) Flp-In T-REx HeLa with or without doxycycline (24 h) were imaged using lamin A/C antibody. Arrows indicate abnormal nuclear lamina phenotype-exhibiting cells.

(B) Graph showing percentage cells showing nuclear abnormality during expression of lamin A targeting PISM constructs. Cells were counted manually and presented as mean (box) of four replicates (points) with SD.

(C) Western blot analysis on parental and myc-tagged lamin A targeting PISM (IR1-M high and low activity) Flp-In T-REx HeLa with or without doxycycline (24 h) using antibodies against lamin A/C, Myc, and actin. Long exposure using lamin A/C was used to visualized SUMO-modified lamin A/C and short exposure to monitor unmodified lamin A/C. Data derived from single blots cropped to remove irrelevant lanes (see source data at https://doi.org/10.17632/bsxmfv7stg.1).

forms may not accumulate as they trigger apoptosis in IPS cells but not HeLas.

DISCUSSION

SENP6 is one of a small number of SUMO-specific proteases critical for maintaining SUMO homeostasis. Along with SENP7, it has preference for cleavage of isopeptide bonds between two SUMO moieties and cleaves linkages between SUMO and substrates less efficiently.[20,21] The favored substrate of SENP6 is therefore SUMO chains. It would thus be expected that SENP6 depletion would lead to the accumulation of SUMO chains attached to at least a subset of protein substrates. A slice-by-slice MS analysis was employed to identify potential SENP6 substrates based on their increased apparent MW in SDS-PAGE gels caused by SUMO chain growth when SENP6 is depleted. In these experiments, the clear outliers were the lamin family of intermediate filaments, which not only showed highly significant shifts up through the gel but also accumulated relatively large proportions of cellular SUMO upon SENP6 depletion. During normal cell growth A- and B-type lamins form a meshwork inside the nuclear membrane that maintains nuclear integrity and plays a role in many nuclear processes. A- and C-type lamins are identical for most of their length as they are expressed from the same *LMNA* gene but have different C termini as a product of alternative splicing. B-type lamins are expressed from two different *LMNB1* and *LMNB2* genes.[45,46] Mutations in lamins are the cause of many genetic diseases

collectively termed laminopathies. Depletion of SENP6 leads to the accumulation of highly SUMO-modified lamins and changes to nuclear structure and lamin A/C distribution. The abnormally shaped nuclei and disrupted lamin A/C staining observed after SENP6 depletion (Figure 4) are strikingly similar to the phenotypes observed in certain forms of laminopathies. Two of the three lysine residues identified as SUMO acceptors in lamin A/C (Figures 3 and 4) were immediately adjacent to sites at which mutations give rise to Emery-Dreifuss muscular dystrophy and limb girdle muscular dystrophy, two well characterized laminopathies. AlphaFold models of lamin A/C indicate that the sites of laminopathy-causing mutations and SUMO modification would likely disrupt formation of coiled-coil structures required for dimerization, the first step in assembly of the nuclear lamina. It is important to note that, while we demonstrate that hyperSUMOylation of lamins results in changes to nuclear structure that are similar to those observed in certain laminopathies, we are not suggesting that the mutations in lamins associated with laminopathies induce hyperSUMOylation of lamins. Rather, it is likely that amino-acid changes directly cause defects in the assembly of the nuclear lamina.

It is clear from the heatmaps in Figure 3E that, after SENP6 knockdown, SUMO-SUMO branched peptides increase dramatically as one would expect if SENP6 is a chain-specific protease. However, SUMO-lamin branched peptides also increase, and this is not consistent with SENP6 having a strict SUMO-SUMO chain specificity. There are a number of possible explanations for this observation. One is simply that SENP6 chain specificity is not absolute and that, in cells, it can remove a certain amount of SUMO directly from substrates. An alternative possibility is that, under normal conditions, other SUMO proteases that function to remove single SUMO molecules from substrates are inhibited from
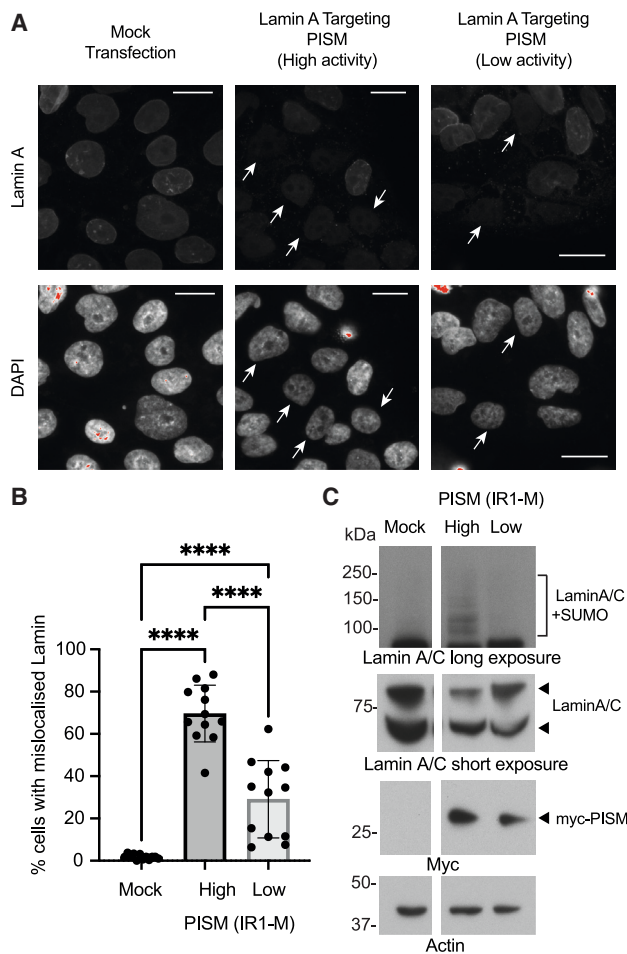
A

B

C

Figure 7. Transfecting IPS cells with lamin A targeting PISM results in diffusion of lamin A

(A) Human IPS cells (hIPSCs) transfected with myc-tagged lamin A targeting PISM mRNA or mock transfected and fixed after 24 h. Cells were imaged using lamin A/C antibody. Arrows indicate diffused nuclear lamina phenotype-exhibiting cells.

(B) Graph showing percentage of cells with mis-localized lamin A. Four counts per replicate were performed and columns show the average of all 12 counts across three replicate experiments. Error bars show SD, and the results of one-way ANOVA are summarized above.

(C) Western blot analysis on mock and myc-tagged lamin A targeting PISM mRNA transfected hIPSCs using antibodies against lamin A/C, Myc, and actin. Long exposure using lamin A/C was used to visualize SUMO-modified lamin A/C and short exposure for unmodified lamin A/C. Data derived from single blots cropped to remove irrelevant lanes (see source data at https://doi.org/10.17632/bsxmfv7stg.1).

doing so by the accumulation of SUMO polymers. This could either be through direct physical impediment of the attached SUMO chain or by abundant SUMO-SUMO linkages competing with the SUMO-substrate linkages for finite protease activity.

Studies employing SENP6 knockdown have identified multiple roles for SENP6, including kinetochore assembly,[25,27] PML body dynamics,[24] and genome maintenance.[47] More recently, two large-scale proteomic analyses have identified many proteins that show increased SUMO modification after SENP6 depletion and, based on groups of proteins modified, showed that SENP6 facilitates assembly of the constitutive centromere-associated network[26] and regulates protein recruitment to chromatin for genome maintenance and chromosome dynamics.[28] Our study confirmed some of these findings and also revealed that lamins are among the most significant responders in terms of SUMO modification in the absence of SENP6. However, given the large number of SUMO substrates and therefore the potentially pleiotropic nature of SENP6 depletion, it was difficult to conclude that the laminopathy-like phenotype we observe after SENP6 depletion is a direct consequence of the accumulation of SUMO on lamins. To address this problem, we developed PISM, in which a lamin A/C targeting DARPin is linked to a SUMO E3 ligase module. This enabled specific, on-demand modification of endogenous lamin A/C. Using this approach, we demonstrated that SUMO modification of lamin A/C recapitulates the damage to nuclear structure and abnormal lamin A/C staining that is manifest after SENP6 depletion (Figures 5 and 6) and that is typical of some laminopathies. We believe this approach can relatively easily be adapted to target SUMOylation of other nuclear substrates and the SUMO E3 ligase module could be fused to other specific binding entities such as nanobodies.

It has been demonstrated previously that lamin A/C can be SUMO modified,[48–51] but, in these cases, laminopathy-causing mutations located close to the lysine acceptor blocked SUMO modification. Here we show that, under normal growth conditions, lamin A/C SUMOylation is undetectable by anti-lamin A/C western blot from crude cell extracts (Figures 5, 6, and 7), which suggests that, under normal growth conditions, it is not highly SUMOylated. This deSUMOylated state is presumably due to the action of SENP6, as depletion of the protease leads to a dramatic increase in SUMO-modified lamin A/C, which becomes detectable by western blot from crude cell extracts (Figures 5, 6, and 7). This is remarkable because the SUMOylated forms of very few substrates can be detected in this way and suggests lamins accumulate relatively large amounts of SUMO when SENP6 levels are reduced. At present, it is not known if SUMO modification of lamins under normal growth conditions has a specific function, and the generally low levels observed in non-synchronized cells may reflect a requirement only at a specific stage of the cell cycle. If this is the case, then the role of SENP6 may be to remove SUMO from lamins after it has performed its putative cell-cycle-associated task. Alternatively, it may be that the SUMO modification is entirely adventitious, resulting from the action of nuclear-localized SUMO modification machinery. Here, the function of SENP6 could be to continually erase the SUMO modification mark from the nuclear lamina to prevent SUMO-induced changes to nuclear structure.

Limitations of the study

The method described here to identify SUMO substrates by changes to their apparent MW relies on good enrichment of the SUMO-modified forms of proteins from cell extracts containing both modified and unmodified proteins. For any protein, contamination of the SUMO-enriched samples with unmodified counterparts will artificially lower the apparent MW calculation and would also suppress the magnitude of the differential in

apparent MW between experimental conditions. Nickel NTA affinity chromatography was employed in this study due to the ability to purify 6His-SUMO2 under denaturing conditions, which deactivates the SUMO proteases that would otherwise deconjugate substrates. However, it has the disadvantage of relatively high levels of non-specific binding for some proteins (for examples, see emerin and lamin A/C above). Thus, we think the sensitivity of this gel-based method for monitoring changes to the apparent MW of SUMOylated proteins would be increased by using a higher-stringency SUMO purification strategy such as the previously employed tandem affinity purification (TAP) tag[52] or 10-histidine tag combined with more stringent washes and further purification steps.[53]

While our slice-by-slice proteomic analysis indicated that SUMO modification of lamins increased dramatically after SENP6 knockdown, it was not possible to ascribe the accompanying laminopathy-like phenotype to SUMO modification of lamins as SENP6 depletion affected the SUMOylation status of other proteins. In an attempt to link the phenotypical changes to the modification state of lamins, we developed PISM, which allows targeted SUMO modification of any substrate. In this approach, we create an engineered SUMO E3 ligase where substrate specificity is provided by a DARPin recognizing lamin A/C and E3 ligase activity is provided by the catalytic module of RanBP2. While the lamin A targeting DARPin does not disrupt lamin A assembly *in vivo*,[38] its epitope was not mapped. Thus, it is unknown where on lamin A the DARPin binds. As with most SUMO substrates, only a small proportion of lamin A/C is modified at the steady state and this proportion increases after treatment with the PISM construct. Even in this situation, only a small proportion of the total protein is modified, but this is probably enough to disrupt formation of the higher order assemblies of lamin A/C that form the nuclear lamina.

While the high affinity and selectivity of the DARPin for lamin A/C should ensure specific recognition of the lamin target, we cannot completely rule out "off-target" effects. Indeed, SUMO modification of lamin B, which is also a component of the nuclear lamina, was increased with PISM expression, but other closely associated proteins, such as emerin, are not modified. Thus our western blotting experiments indicate that PISM is rather specific, but a limitation of the study is that we cannot absolutely exclude the possibility that other proteins contribute to the observed phenotype.

STAR★METHODS

Detailed methods are provided in the online version of this paper and include the following:

- KEY RESOURCES TABLE
- RESOURCE AVAILABILITY
  - Lead contact
  - Materials availability
  - Data and code availability
- EXPERIMENTAL MODEL AND STUDY PARTICIPANT DETAILS
- METHOD DETAILS
  - Cloning of lamin targeting PISM

  - siRNA transfection
  - DNA transfection
  - mRNA transfection (HeLa, U2OS ChiPS4 cells)
  - Polyacrylamide gel electrophoresis (SDS-PAGE)
  - Western blotting
  - Proteomic sample Preparation
  - Mass spectrometry analysis
  - MS data processing
  - Data normalization and apparent MW calculation
  - Data filtering and statistical analysis
  - % Global protein intensity change
  - Immunofluorescence
  - *In vitro* transcription of PISM mRNAs
  - Alphafold model of a human lamin A dimer
- QUANTIFICATION AND STATISTICAL ANALYSIS

REFERENCES

1. Tatham, M.H., Jaffray, E., Vaughan, O.A., Desterro, J.M., Botting, C.H., Naismith, J.H., and Hay, R.T. (2001). Polymeric chains of SUMO-2 and SUMO-3 are conjugated to protein substrates by SAE1/SAE2 and Ubc9. J. Biol. Chem. *276*, 35368–35374. https://doi.org/10.1074/jbc.M104214200.

2. Matic, I., van Hagen, M., Schimmel, J., Macek, B., Ogg, S.C., Tatham, M.H., Hay, R.T., Lamond, A.I., Mann, M., and Vertegaal, A.C.O. (2008). In vivo identification of human small ubiquitin-like modifier polymerization sites by high accuracy mass spectrometry and an in vitro to in vivo strategy. Mol. Cell. Proteomics 7, 132–144. https://doi.org/10.1074/mcp.M700173-MCP200.

3. Cooper, H.J., Tatham, M.H., Jaffray, E., Heath, J.K., Lam, T.T., Marshall, A.G., and Hay, R.T. (2005). Fourier transform ion cyclotron resonance mass spectrometry for the analysis of small ubiquitin-like modifier (SUMO) modification: Identification of lysines in RanBP2 and SUMO targeted for modification during the E3 AutoSUMOylation reaction. Anal. Chem. 77, 6310–6319. https://doi.org/10.1021/ac058019d.

4. Golebiowski, F., Matic, I., Tatham, M.H., Cole, C., Yin, Y., Nakamura, A., Cox, J., Barton, G.J., Mann, M., and Hay, R.T. (2009). System-Wide Changes to SUMO Modifications in Response to Heat Shock. Sci. Signal. 2, ra24, ARTN ra24. https://doi.org/10.1126/scisignal.2000282.

5. Hendriks, I.A., D'Souza, R.C.J., Yang, B., Verlaan-de Vries, M., Mann, M., and Vertegaal, A.C.O. (2014). Uncovering global SUMOylation signaling networks in a site-specific manner. Nat. Struct. Mol. Biol. 21, 927–936. https://doi.org/10.1038/nsmb.2890.

6. Desterro, J.M., Rodriguez, M.S., Kemp, G.D., and Hay, R.T. (1999). Identification of the enzyme required for activation of the small ubiquitin-like protein SUMO-1. J. Biol. Chem. 274, 10618–10624. https://doi.org/10.1074/jbc.274.15.10618.

7. Bernier-Villamor, V., Sampson, D.A., Matunis, M.J., and Lima, C.D. (2002). Structural basis for E2-mediated SUMO conjugation revealed by a complex between ubiquitin-conjugating enzyme Ubc9 and RanGAP1. Cell 108, 345–356. https://doi.org/10.1016/S0092-8674(02)00630-X.

8. Hecker, C.M., Rabiller, M., Haglund, K., Bayer, P., and Dikic, I. (2006). Specification of SUMO1- and SUMO2-interacting motifs. J. Biol. Chem. 281, 16117–16127. https://doi.org/10.1074/jbc.M512757200.

9. Song, J., Durrin, L.K., Wilkinson, T.A., Krontiris, T.G., and Chen, Y. (2004). Identification of a SUMO-binding motif that recognizes SUMO-modified proteins. Proc. Natl. Acad. Sci. USA 101, 14373–14378.

10. Sun, H.Y., and Hunter, T. (2012). Poly-Small Ubiquitin-like Modifier (PolySUMO)-binding Proteins Identified through a String Search. J. Biol. Chem. 287, 42071–42083. https://doi.org/10.1074/jbc.M112.410985.

11. Song, J., Zhang, Z., Hu, W., and Chen, Y. (2005). Small ubiquitin-like modifier (SUMO) recognition of a SUMO binding motif - A reversal of the bound orientation. J. Biol. Chem. 280, 40122–40129. https://doi.org/10.1074/jbc.M507059200.

12. He, X., Riceberg, J., Soucy, T., Koenig, E., Minissale, J., Gallery, M., Bernard, H., Yang, X., Liao, H., Rabino, C., et al. (2017). Probing the roles of SUMOylation in cancer cell biology by using a selective SAE inhibitor. Nat. Chem. Biol. 13, 1164–1171. https://doi.org/10.1038/Nchembio.2463.

13. Hickey, C.M., Wilson, N.R., and Hochstrasser, M. (2012). Function and regulation of SUMO proteases. Nat. Rev. Mol. Cell Biol. 13, 755–766. https://doi.org/10.1038/nrm3478.

14. Shin, E.J., Shin, H.M., Nam, E., Kim, W.S., Kim, J.H., Oh, B.H., and Yun, Y. (2012). DeSUMOylating isopeptidase: a second class of SUMO protease. EMBO Rep. 13, 339–346. https://doi.org/10.1038/embor.2012.3.

15. Schulz, S., Chachami, G., Kozaczkiewicz, L., Winter, U., Stankovic-Valentin, N., Haas, P., Hofmann, K., Urlaub, H., Ovaa, H., Wittbrodt, J., et al. (2012). Ubiquitin-specific protease-like 1 (USPL1) is a SUMO isopeptidase with essential, non-catalytic functions. EMBO Rep. 13, 930–938. https://doi.org/10.1038/embor.2012.125.

16. Li, Y., Varejão, N., and Reverter, D. (2022). Structural basis for the SUMO protease activity of the atypical ubiquitin-specific protease USPL1. Nat. Commun. 13, 1819, ARTN 1819. https://doi.org/10.1038/s41467-022-29485-0.

17. Hay, R.T. (2007). SUMO-specific proteases: a twist in the tail. Trends Cell Biol. 17, 370–376. https://doi.org/10.1016/j.tcb.2007.08.002.

18. Shen, L.N., Dong, C., Liu, H., Naismith, J.H., and Hay, R.T. (2006). The structure of SENP1-SUMO-2 complex suggests a structural basis for discrimination between SUMO paralogues during processing. Biochem. J. 397, 279–288. https://doi.org/10.1042/Bj20052030.

19. Reverter, D., and Lima, C.D. (2006). Structural basis for SENP2 protease interactions with SUMO precursors and conjugated substrates. Nat. Struct. Mol. Biol. 13, 1060–1068. https://doi.org/10.1038/nsmb1168.

20. Mukhopadhyay, D., Ayaydin, F., Kolli, N., Tan, S.H., Anan, T., Kametaka, A., Azuma, Y., Wilkinson, K.D., and Dasso, M. (2006). SUSP1 antagonizes formation of highly SUMO2/3-conjugated species. J. Cell Biol. 174, 939–949. https://doi.org/10.1083/jcb.200510103.

21. Lima, C.D., and Reverter, D. (2008). Structure of the Human SENP7 Catalytic Domain and Poly-SUMO Deconjugation Activities for SENP6 and SENP7. J. Biol. Chem. 283, 32045–32055. https://doi.org/10.1074/jbc.M805655200.

22. Alegre, K.O., and Reverter, D. (2014). Structural insights into the SENP6 Loop1 structure in complex with SUMO2. Protein Sci. 23, 433–441. https://doi.org/10.1002/pro.2425.

23. Shen, L.N., Geoffroy, M.C., Jaffray, E.G., and Hay, R.T. (2009). Characterization of SENP7, a SUMO-2/3-specific isopeptidase. Biochem. J. 421, 223–230. https://doi.org/10.1042/Bj20090246.

24. Hattersley, N., Shen, L., Jaffray, E.G., and Hay, R.T. (2011). The SUMO protease SENP6 is a direct regulator of PML nuclear bodies. Mol. Biol. Cell 22, 78–90. https://doi.org/10.1091/mbc.E10-06-0504.

25. Mukhopadhyay, D., Arnaoutov, A., and Dasso, M. (2010). The SUMO protease SENP6 is essential for inner kinetochore assembly. J. Cell Biol. 188, 681–692. https://doi.org/10.1083/jcb.200909008.

26. Liebelt, F., Jansen, N.S., Kumar, S., Gracheva, E., Claessens, L.A., Verlaan-de Vries, M., Willemstein, E., and Vertegaal, A.C.O. (2019). The poly-SUMO2/3 protease SENP6 enables assembly of the constitutive centromere-associated network by group deSUMOylation. Nat. Commun. 10, 3987, ARTN 3987. https://doi.org/10.1038/s41467-019-11773-x.

27. Mitra, S., Bodor, D.L., David, A.F., Abdul-Zani, I., Mata, J.F., Neumann, B., Reither, S., Tischer, C., and Jansen, L.E.T. (2020). Genetic screening identifies a SUMO protease dynamically maintaining centromeric chromatin. Nat. Commun. 11, 501, ARTN 501. https://doi.org/10.1038/s41467-019-14276-x.

28. Wagner, K., Kunz, K., Piller, T., Tascher, G., Hölper, S., Stehmeier, P., Keiten-Schmitz, J., Schick, M., Keller, U., and Müller, S. (2019). The SUMO Isopeptidase SENP6 Functions as a Rheostat of Chromatin Residency in Genome Maintenance and Chromosome Dynamics. Cell Rep. 29, 480–494.e5. https://doi.org/10.1016/j.celrep.2019.08.106.

29. Schick, M., Zhang, L., Maurer, S., Maurer, H.C., Isaakidis, K., Schneider, L., Patra, U., Schunck, K., Rohleder, E., Hofstetter, J., et al. (2022). Genetic alterations of the SUMO isopeptidase SENP6 drive lymphomagenesis and genetic instability in diffuse large B-cell lymphoma. Nat. Commun. 13, 281, ARTN 281. https://doi.org/10.1038/s41467-021-27704-8.

30. Tatham, M.H., Matic, I., Mann, M., and Hay, R.T. (2011). Comparative Proteomic Analysis Identifies a Role for SUMO in Protein Quality Control. Sci. Signal. 4, rs4, ARTN rs4. https://doi.org/10.1126/scisignal.2001484.

31. Bruderer, R., Tatham, M.H., Plechanovova, A., Matic, I., Garg, A.K., and Hay, R.T. (2011). Purification and identification of endogenous polySUMO conjugates. EMBO Rep. 12, 142–148. https://doi.org/10.1038/embor.2010.206.

32. Tatham, M.H., Geoffroy, M.C., Shen, L., Plechanovova, A., Hattersley, N., Jaffray, E.G., Palvimo, J.J., and Hay, R.T. (2008). RNF4 is a poly-SUMO-specific E3 ubiquitin ligase required for arsenic-induced PML degradation. Nat. Cell Biol. 10, 538–546. https://doi.org/10.1038/ncb1716.

33. Malashicheva, A., and Perepelina, K. (2021). Diversity of Nuclear Lamin A/C Action as a Key to Tissue-Specific Regulation of Cellular Identity in Health and Disease. Front. Cell Dev. Biol. 9, 761469, ARTN 761469. https://doi.org/10.3389/fcell.2021.761469.

34. Shin, J.Y., and Worman, H.J. (2022). Molecular Pathology of Laminopathies. Annu. Rev. Pathol. *17*, 159–180. https://doi.org/10.1146/annurev-pathol-042220-034240.

35. Rojas-Fernandez, A., Plechanovová, A., Hattersley, N., Jaffray, E., Tatham, M.H., and Hay, R.T. (2014). SUMO Chain-Induced Dimerization Activates RNF4. Mol. Cell. *53*, 880–892. https://doi.org/10.1016/j.molcel.2014.02.031.

36. Ibrahim, A.F.M., Shen, L., Tatham, M.H., Dickerson, D., Prescott, A.R., Abidi, N., Xirodimas, D.P., and Hay, R.T. (2020). Antibody RING-Mediated Destruction of Endogenous Proteins. Mol. Cell. *79*, 155–166.e9. https://doi.org/10.1016/j.molcel.2020.04.032.

37. Binz, H.K., Stumpp, M.T., Forrer, P., Amstutz, P., and Plückthun, A. (2003). Designing repeat proteins: Well-expressed, soluble and stable proteins from combinatorial libraries of consensus ankyrin repeat proteins. J. Mol. Biol. *332*, 489–503. https://doi.org/10.1016/S0022-2836(03)00896-9.

38. Zwerger, M., Roschitzki-Voser, H., Zbinden, R., Denais, C., Herrmann, H., Lammerding, J., Grütter, M.G., and Medalia, O. (2015). Altering lamina assembly reveals lamina-dependent and -independent functions for A-type lamins. J. Cell Sci. *128*, 3607–3620. https://doi.org/10.1242/jcs.171843.

39. Pichler, A., Gast, A., Seeler, J.S., Dejean, A., and Melchior, F. (2002). The nucleoporin RanBP2 has SUMO1 E3 ligase activity. Cell *108*, 109–120. https://doi.org/10.1016/S0092-8674(01)00633-X.

40. Pichler, A., Knipscheer, P., Oberhofer, E., van Dijk, W.J., Körner, R., Olsen, J.V., Jentsch, S., Melchior, F., and Sixma, T.K. (2005). SUMO modification of the ubiquitin-conjugating enzyme E2-25K. Nat. Struct. Mol. Biol. *12*, 264–269. https://doi.org/10.1038/nsmb903.

41. Reverter, D., and Lima, C.D. (2005). Insights into E3 ligase activity revealed by a SUMO-RanGAP1-Ubc9-Nup358 complex. Nature *435*, 687–692. https://doi.org/10.1038/nature03588.

42. Tatham, M.H., Kim, S., Jaffray, E., Song, J., Chen, Y., and Hay, R.T. (2005). Unique binding interactions among Ubc9, SUMO and RanBP2 reveal a mechanism for SUMO paralog selection. Nat. Struct. Mol. Biol. *12*, 67–74. https://doi.org/10.1038/nsmb878.

43. Pichler, A., Knipscheer, P., Saitoh, H., Sixma, T.K., and Melchior, F. (2004). The RanBP2 SUMO E3 ligase is neither HECT- nor RING-type. Nat. Struct. Mol. Biol. *11*, 984–991. https://doi.org/10.1038/nsmb834.

44. Weisshaar, S.R., Keusekotten, K., Krause, A., Horst, C., Springer, H.M., Göttsche, K., Dohmen, R.J., and Praefcke, G.J.K. (2008). Arsenic trioxide stimulates SUMO-2/3 modification leading to RNF4-dependent proteolytic targeting of PML. FEBS Lett. *582*, 3174–3178. https://doi.org/10.1016/j.febslet.2008.08.008.

45. Dittmer, T.A., and Misteli, T. (2011). The lamin protein family. Genome Biol. *12*, 222, ARTN 222. https://doi.org/10.1186/gb-2011-12-5-222.

46. de Leeuw, R., Gruenbaum, Y., and Medalia, O. (2018). Nuclear Lamins: Thin Filaments with Major Functions. Trends Cell Biol. *28*, 34–45. https://doi.org/10.1016/j.tcb.2017.08.004.

47. Gibbs-Seymour, I., Oka, Y., Rajendra, E., Weinert, B.T., Passmore, L.A., Patel, K.J., Olsen, J.V., Choudhary, C., Bekker-Jensen, S., and Mailand, N. (2015). Ubiquitin-SUMO Circuitry Controls Activated Fanconi Anemia ID Complex Dosage in Response to DNA Damage. Mol. Cell. *57*, 150–164. https://doi.org/10.1016/j.molcel.2014.12.001.

48. Zhang, Y.Q., and Sarge, K.D. (2008). Sumoylation regulates lamin A function and is lost in lamin A mutants associated with familial cardiomyopathies. J. Cell Biol. *182*, 35–39. https://doi.org/10.1083/jcb.200712124.

49. Kelley, J.B., Datta, S., Snow, C.J., Chatterjee, M., Ni, L., Spencer, A., Yang, C.S., Cubeñas-Potts, C., Matunis, M.J., and Paschal, B.M. (2011). The Defective Nuclear Lamina in Hutchinson-Gilford Progeria Syndrome Disrupts the Nucleocytoplasmic Ran Gradient and Inhibits Nuclear Localization of Ubc9. Mol. Cell Biol. *31*, 3378–3395. https://doi.org/10.1128/Mcb.05087-11.

50. Boudreau, É., Labib, S., Bertrand, A.T., Decostre, V., Bolongo, P.M., Sylvius, N., Bonne, G., and Tesson, F. (2012). Lamin A/C Mutants Disturb Sumo1 Localization and Sumoylation in Vitro and in Vivo. PLoS One *7*, e45918, ARTN e45918. https://doi.org/10.1371/journal.pone.0045918.

51. Simon, D.N., Domaradzki, T., Hofmann, W.A., and Wilson, K.L. (2013). Lamin A tail modification by SUMO1 is disrupted by familial partial lipodystrophy-causing mutations. Mol. Biol. Cell *24*, 342–350. https://doi.org/10.1091/mbc.E12-07-0527.

52. Golebiowski, F., Tatham, M.H., Nakamura, A., and Hay, R.T. (2010). High-stringency tandem affinity purification of proteins conjugated to ubiquitin-like moieties. Nat. Protoc. *5*, 873–882. https://doi.org/10.1038/nprot.2010.40.

53. Hendriks, I.A., Lyon, D., Young, C., Jensen, L.J., Vertegaal, A.C.O., and Nielsen, M.L. (2017). Site-specific mapping of the human SUMO proteome reveals co-modification with phosphorylation. Nat. Struct. Mol. Biol. *24*, 325–336. https://doi.org/10.1038/nsmb.3366.

54. Perez-Riverol, Y., Bai, J., Bandla, C., García-Seisdedos, D., Hewapathirana, S., Kamatchinathan, S., Kundu, D.J., Prakash, A., Frericks-Zipper, A., Eisenacher, M., et al. (2022). The PRIDE database resources in 2022: a hub for mass spectrometry-based proteomics evidences. Nucleic Acids Res. *50*, D543–D552. https://doi.org/10.1093/nar/gkab1038.

55. Ludwig, T.E., Levenstein, M.E., Jones, J.M., Berggren, W.T., Mitchen, E.R., Frane, J.L., Crandall, L.J., Daigh, C.A., Conard, K.R., Piekarczyk, M.S., et al. (2006). Derivation of human embryonic stem cells in defined conditions. Nat. Biotechnol. *24*, 185–187. https://doi.org/10.1038/nbt1177.

56. Sloan, E., Tatham, M.H., Groslambert, M., Glass, M., Orr, A., Hay, R.T., and Everett, R.D. (2015). Analysis of the SUMO2 Proteome during HSV-1 Infection. PLoS Pathog. *11*, e1005059, ARTN e1005059. https://doi.org/10.1371/journal.ppat.1005059.

57. Cox, J., and Mann, M. (2008). MaxQuant enables high peptide identification rates, individualized p.p.b.-range mass accuracies and proteome-wide protein quantification. Nat. Biotechnol. *26*, 1367–1372. https://doi.org/10.1038/nbt.1511.

58. Evans, R., O'Neill, M., Pritzel, A., Antropova, N., Senior, A., Green, T., Žídek, A., Bates, R., Blackwell, S., Yim, J., et al. (2022). Protein Complex Prediction with AlphaFold-Multimer. Preprint at bioRxiv, 2021.2010.2004.463034. https://doi.org/10.1101/2021.10.04.463034.

59. Mirdita, M., Schütze, K., Moriwaki, Y., Heo, L., Ovchinnikov, S., and Steinegger, M. (2022). ColabFold: making protein folding accessible to all. Nat. Methods *19*, 679–682. https://doi.org/10.1038/s41592-022-01488-1.

STAR★METHODS

KEY RESOURCES TABLE

REAGENT or RESOURCE	SOURCE	IDENTIFIER
Antibodies		
Mouse anti-lamin A/C	Sigma Aldrich	SAB4200236; RRID:AB_10743057
Mouse anti-Myc Tag	Cell Signaling Technologies	2276; RRID:AB_331783
Rabbit anti-lamin A/C	Abcam	ab227176
Rabbit anti-lamin B1	Abcam	ab8982; RRID:AB_1640627
Sheep anti-SUMO2	In house generated	N/A
Chemicals, peptides, and recombinant proteins		
Doxycycline Hydrochloride	Sigma-Aldrich	D3447
SUMO inhibitor ML792	Sigma Aldrich	1644342-14-2
KOD Hot Start DNA Polymerase	Merck Millipore	71086
Protease Inhibitor cocktail	Roche	11836170001
DMEM+Glutamax^{TM}-1 medium	Life Technologies	61965–026
Minimum essential Medium + Eagle's Salts	Thermo Fisher	11090081
L-Glutamine	Lonza	12-611F
Fetal Bovine Serum	Labtech.com	FCS-SA
siRNA targeting SENP6 (ON-TARGETplus; SMARTpool)	HorizonDiscovery	L-006044-00-0010
Critical commercial assays		
Lipofectamine 3000	Life Technologies	L3000015
Lipofectamine RNAiMAX	Life Technologies	13778150
mMESSAGE mMACHINE T7 ULTRA Transcription Kit	Thermo Fisher	AM1345
MEGAclear Transcription Clean-Up Kit	Thermo Fisher	AM1908
QIAquick MinElute Gel Extraction Kit	QIAGEN	28604
Pierce BCA Protein Assay Kit	Thermo Fisher	23225
jetMESSENGER	VWR	101000005
ECL Western blotting substrate	Thermo Fisher	32209
Deposited data		
Mass spectrometry	https://www.ebi.ac.uk/pride/	PXD036743
Western Blot images	https://data.mendeley.com/	10.17632/bsxmfv7stg.1
Experimental models: Cell lines		
ChiPS4 cells (hIPSCs)	Cellartis (Takara)	N/A
HeLa	ATCC	CCL-2
HeLa Flp-in/T Rex	Thermo Fisher	R71407
HeLa Flp-in/T Rex Non-targeting Darpin PISM (IR1-*M*-IR2)	This study	N/A
HeLa Flp-in/T Rex lamin A-targeting Darpin PISM (IR1-*M*-IR2)	This study	N/A
HeLa Flp-in/T Rex lamin A-targeting Darpin PISM (IR1-*M*-IR2) mutant	This study	N/A
HeLa Flp-in/T Rex lamin A-targeting Darpin PISM (IR1-M) High activity	This study	N/A
HeLa Flp-in/T Rex lamin A-targeting Darpin PISM (IR1-M) mutant – low activity	This study	N/A
GFP-AID-SENP6 HeLa	Mitra et al.[27]	https://doi.org/10.1038/s41467-019-14276-x

Continued

REAGENT or RESOURCE	SOURCE	IDENTIFIER
Oligonucleotides		
Oligonucleotides see Table S1	Integrated DNA Technologies, Inc.	N/A
Recombinant DNA		
pOG44	Invitrogen	V600520
pCDNA5 FRT/TO Non-targeting Darpin PISM (IR1-*M*-IR2)	This study	N/A
pCDNA5 FRT/TO lamin A-targeting Darpin PISM (IR1-*M*-IR2)	This study	N/A
pCDNA5 FRT/TO lamin A-targeting Darpin PISM (IR1-*M*-IR2) mutant	This study	N/A
pCDNA5 FRT/TO lamin A-targeting Darpin PISM (IR1-M) High activity	This study	N/A
pCDNA5 FRT/TO lamin A-targeting Darpin PISM (IR1-M) mutant – low activity	This study	N/A
Software and algorithms		
MaxQuant	MPI Munich	https://www.maxquant.org
Perseus	MPI Munich	https://www.maxquant.org/perseus/
Graphpad PRISM v9	GraphPad Software	https://www.graphpad.com/
Alphafold	Deepmind	https://www.deepmind.com/

RESOURCE AVAILABILITY

Lead contact
Further information and requests for resources and reagents should be directed to and will be fulfilled by the lead contact, Ronald T. Hay (R.T.Hay@dundee.ac.uk).

Materials availability
Reagents generated in this study are available from the lead contact with a completed materials transfer agreement.

Data and code availability
Original Western blot images have been deposited at Mendeley. Accession number is in the key resources table. Mass spectrometry proteomics data have been deposited at ProteomeXchange Consortium via the PRIDE[54] partner repository and are publicly available as of the date of publication. Accession number are listed in the key resources table. This paper does not report original code. Any additional information required to reanalyse the data reported in this paper is available from the lead contact upon request.

EXPERIMENTAL MODEL AND STUDY PARTICIPANT DETAILS

6-His-SUMO2 HeLa were cultured in DMEM+Glutamax-1 medium supplemented with 10% Calf Serum and penicillin-streptomycin. GFP-AID-SENP6 HeLa (Mitra, Sreyoshi & Bodor, Dani & David, Ana & Mata, João & Neumann, Beate & Reither, Sabine & Tischer, Christian & Jansen, Lars. (2019). Genetic screening identifies a SUMO protease dynamically maintaining centromeric chromatin and the associated centromere complex. 10.1101/620088.) were cultured in DMEM+Glutamax-I medium supplemented with 10% Fetal Bovine Serum and penicillin-streptomycin, Neomycin (500 μg/ml), Blasticidin (1 μg/ml) and Puromycin (1 μg/ml). HeLa, Flp-in/T.rex cells were cultured in Minimum essential Medium + Eagle's salts supplemented with L-Glutamine, 10% Calf Serum and penicillin-streptomycin. HeLa Flp-in/T Rex grown in monolayer were transfected with each of the non-targeting or lamin A targeting-wild-type or mutant PISM vectors, along with the Flp recombinase vector pOG44, using Lipofectamine 3000 according to the manufacturer's instructions and selected with hygromycin at 100 μg/mL. Thereafter, stable cell populations were maintained in growth medium containing hygromycin (50 μg/mL) and blasticidin (5 μg/mL).

Human Induced pluripotent stem cells (hiPSCs) culture and transfection protocols. Cell lines were maintained in TESR medium[55] containing FGF2 (Peprotech, 30 ng/mL) and noggin (Peprotech, 10 ng/mL) on growth factor reduced geltrex basement membrane extract (Life Technologies, 10 μg/cm²) coated dishes at 37°C in a humidified atmosphere of 5% CO₂ in air. Cells were routinely passaged twice a week as single cells using TrypLE select (Life Technologies) and replated in TESR medium that was further supplemented with the Rho kinase inhibitor Y27632 (Tocris, 10 μM). Twenty-four hours after replating Y27632 was removed from the culture medium.

METHOD DETAILS

Cloning of lamin targeting PISM

pCDNA5 FRT/TO vector containing GFP-nanobody-RanBP2 (IR1-*M*-IR2) was as described.[36] Substitution of GFP-nanobody sequence with lamin-targeting Darpin[38] sequence was made using gBLOCKS obtained from Integrated DNA Technologies (https://eu.idtdna.com/). gBlock were PCR amplified using forward and specific reverse primers. gBlock and subsequent vectors were validated by sequencing. Two mutations L2651A and L2653A were introduced into RanBP2 (IR1-*M*-IR2) lamin A targeting Darpin-PISM and mutations were confirmed by sequencing. Removal of IR2 domain of RanBP2 was performed using PCR amplification with primers. Elimination was validated by sequencing.

siRNA transfection

Cells were transfected with a siRNA targeting SENP6 (ON-TARGETplus; SMARTpool). Cells were seeded one day prior to planned transfection (to reach about 80–90% confluency the next day). Lipofectamine siRNAmax was used as transfection reagent according to manufacturer instructions with final siRNA concentration of 10nM. Cells were incubated up to 72h post transfection (specific times indicated for specific experiments). Non-targeting siRNA was used as a control.

DNA transfection

Cells were seeded a one day prior to planned transfection (to reach about 80–90% confluency the next day). Lipofectamine 3000 was used as transfection reagent according to manufacturer instructions. Cells were incubated for 24h post transfection and specific selection was performed.

mRNA transfection (HeLa, U2OS ChiPS4 cells)

Cells were seeded a one day prior to planned transfection (to reach about 80–90% confluency the next day). jetMESSENGER was used as transfection reagent according to manufacturer instruction with amounts of mRNA optimised (50ng of mRNA per 500ul of culture media per well of 24 well plate). Cells were incubated for up to 24h post transfection (specific times indicated for specific experiments). ChiPS4 cells were transfected using a Neon electroporation system (Thermo Fisher Scientific) with 10 μL tips. Briefly, ChiPS4 cells were dispersed to single cells as described before then 0.75×10^6 cells were collected by centrifugation at 300xg for 2 min and resuspended in 11 μL of electroporation buffer R containing 1 μg of specific mRNAs. Electroporation was performed at 1150 V, 1 pulse, 30 mSec and cells plated in mTESR containing Y27632. Cells were collected and further analyzed by immunofluorescence or western blotting.

Polyacrylamide gel electrophoresis (SDS-PAGE)

All polyacrylamide gel electrophoresis was performed using precast NuPAGE 4 to 12%, Bis-Tris, 1.0 mm, Protein Gels in Novex mini gel kits at 90-180V in MOPS buffer and then transferred using iBlot 2 gel transfer device or stained using Coomassie blue staining.

Western blotting

Fractionated proteins were transferred using iBlot 2 gel transfer device. After transfer membranes were blocked for 40-60min in 5% milk in TBS-T (Tris-Buffered Saline +0.1% TWEEN 20) then washed 3 times with TBS-T. Membranes were then incubated with primary antibody in 5% BSA solution in TBS-T overnight at 4°C. Membranes were washed 3 times with TBS-T and incubated with secondary antibody in 5% milk in TBS-T for 1h at room temperature. Membranes were washed 3 times with TBS-T then developed by incubation with ECL substrate for 2min and exposure to X-ray films.

Proteomic sample Preparation

6His-SUMO2 HeLa cells were maintained as described above. SiRNA knockdown of SENP6 was performed in triplicate as described above. Cells were harvested by washing culture dishes with PBS containing 100mM Iodoacetamide then scraped and pelleted by centrifugating at 300g for 10 min at 4°C. Input samples were collected at this stage for Western blotting. Cells were lyzed in 5x cell pellet weight of lysis buffer; 6 M guanidine-HCl, 100 mM sodium phosphate buffer (pH 8.0), 10 mM Tris-HCl (pH 8.0), 10 mM imidazole, 5 mM 2-mercaptoethanol and frozen down in −80°C. Lysed cells were thawed and DNA was sheared by sonicating (Branson Digital Sonifier) using 3min of 35% amplitude; 20sec pulses plus 20sec intervals on ice. Samples were centrifuged at 4000 rpm for 30 min at 4°C and protein concentration was measured using BCA assay (Pierce). Approximately 32mg of protein from each sample was incubated overnight at 4°C with 100uL packed Ni-NTA agarose beads (equilibrated with Lysis Buffer). Bead supernatant was discarded, and beads washed once with 10 resin volumes of Lysis Buffer, once with 10 resin volumes of Wash Buffer (WB): 8 M urea, 100 mM phosphate buffer pH8.0, 10 mM Tris/HCl pH 8.0, 20 mM imidazole, 5 mM β-mercaptoethanol, complete EDTA free protease inhibitor cocktail and six times with 10 resin volumes of WB at pH6.3. Proteins were eluted from Ni-NTA agarose beads by heating to 70°C for 15 min with 1.2x LDS Sample buffer containing DTT (NuPAGE). Elutions from NiNTA purifications were fractionated by SDS-PAGE (NuPAGE 4–12% acrylamide run in MOPS buffer – Thermo Scientific) along with Precision Plus Protein standards (BioRad). Under these conditions the apparent MW of the protein MW markers have been established (Figure S1A). The gel was washed in 10 mM DTT in 100 mM ABC for 1h followed by washing with 50 mM iodoacetamide in 100 mM ABC in the dark at room

temperature for 1h. The gel was washed with 100mM ABC at room temperature for 15 min and cut into 21 slices numbered 1–21 from high to low MW (Figure S1). Diced gel pieces were destained by shaking in 50 mM ammonium bicarbonate (ABC), 50% acetonitrile (ACN) until all the blue was removed. Pieces were then washed in 20mM ABC, 50% ACN by shaking at room temperature for 15 min, before dehydration with 100% ACN and vortexing at room temperature for 5 min. Excess ACN was removed and the gel pieces dried by leaving tubes open in a fume hood for 10–20 min. Proteins were digested in gel by adding just enough 1ug/mL Trypsin (Promega - Trypsin Gold) in 20 mM ABC, 9% ACN to fully rehydrate the gel pieces and cover them with liquid. Digestions were incubated for 16 h at 37°C. Peptides were eluted with 100% ACN and incubated for 30 min at room temperature. Gel pieces were then incubated for 10min in 5% formic acid (FA) + 50% ACN and the liquid was combined with eluted peptides. Gel pieces were fully dehydrated by adding 100 μL ACN and incubated at room temperature for 10 min with vortexing, and the liquid was collected and combined with previous fractions. The liquid was evaporated using by vacuum centrifugation (45°C) until the samples were just short of dryness. Peptide pellets were resuspended in 35uL 1% FA (or 0.5% acetic acid/0.1% TFA) by incubating at room temperature for 10 min with vortexing.

Mass spectrometry analysis

The method to determine apparent molecular weights in polyacrylamide gels for proteins present in SUMO2 purifications from cells overexpressing tagged forms of SUMO2 has been described previously.[30,31,56] Below is a summary of the procedure adapted for this study.

Two analyses of the peptides on two different LC MS/MS set-ups were undertaken. For each run 25% of the total peptide yield was analyzed and both set-ups used an EASY-Spray ion source (Thermo Fisher Scientific) running a 75 μm × 500 mm EASY-Spray column at 45°C.

Run 1: Q Exactive mass spectrometer (Thermo Fisher Scientific) coupled to an EASY-nLC 1000 (Thermo Fisher Scientific). 150 min gradient using a top 8 data-dependent method; full scan (m/z 300–1800) with resolution R = 70,000 at m/z 200 (after accumulation to a target value of 1,000,000 ions with maximum injection time of 20 ms). The 8 most intense ions were fragmented by HCD and measured with a resolution of R = 35,000 at m/z 200 (target value of 500,000 ions and maximum injection time of 120 ms) and intensity threshold of $2.1x10^4$. Peptide match was set to 'preferred'. Ions were ignored if they had unassigned charge state 1, 8 or >8 and a 25 s dynamic exclusion list was applied.

Run2: Q Exactive Plus mass spectrometer (Thermo Scientific) coupled to a Dionex UltiMate 3000 liquid chromatography system (Thermo Scientific). 105 min gradient using a top 10 data-dependent method; full scan (m/z 300–1800) with resolution R = 70,000 at m/z 200 (after accumulation to a target value of 3,000,000 ions with maximum injection time of 20 ms). The 10 most intense ions were fragmented by HCD and measured with a resolution of R = 35,000 at m/z 200 (target value of 200,000 ions and maximum injection time of 110 ms) and intensity threshold of 2.1x104. Peptide match was set to 'preferred'. Ions were ignored if they had unassigned charge state 1, 7, 8 or >8 and a 60 s dynamic exclusion list was applied.

MS data processing

126 raw data files were generated from each LC-MS/MS run. All 252 raw files were processed together through MaxQuant version 1.6.1.0[57] with each raw file defined by a unique name in the experimental design template to report data for every detected protein in every peptide sample. Two MaxQuant runs were performed: 1 – To monitor peptide intensity of every human protein detected in every peptide sample for the purposes of App. MW calculations. 2 – To search for SUMO-Substrate branched peptides. The UniProt human proteome database (downloaded 19/04/2019) was used as search database with the variable modifications for both runs included Oxidation (M), Acetyl (Protein N-term), GlyGly (K), Phospho (STY) and for the SUMO branched peptide run the SUMO fragments; FRFDGQPINETDTPAQLEMEDEDTIDVFQQQTGG (K) (3852.706 Da), FRFDGQPINETDTPAQLEM(ox)EDEDTIDVFQQQTGG (K) (3868.70 Da), ELGMEEEDVIEVYQEQTGG (K) (2135.92 Da), and ELGM(ox)EEEDVIEVYQEQTGG (K) (2151.92 Da). Carbamidomethyl (C) was set as fixed modification for both. FDR filtering was 1% at all levels except for SUMO sites, which were unfiltered but manually verified by MS/MS annotation. Match between runs was switched off and max missed cleavages by Trypsin/P was set to 3. No peptides with more than 3 modifications were reported. Maximum peptides mass was 10000 Da (Proteome analysis) or 12000 Da (Branched peptide analysis). Raw intensity data and not LFQ was used for downstream processing.

Data normalization and apparent MW calculation

To assign an MW_{App} to a protein in a particular sample it was first necessary to assign an average MW_{App} to each of the 21 slices from the SDS-PAGE gel. This was done using the positions of the upper and lower cuts relative to the MW markers, and using an equation relating apparent MW to distance from the well (retention factor) (see Figures S1B and S1C;[30,31,56]). To calculate an apparent MW for every protein detected in each replicate data from the MaxQuant 'proteinGroups.txt' file was used. Proteins derived from the decoy database, only identified by a modified peptide, or defined as a contaminant were removed prior to downstream processing, and raw intensity values were used in preference to LFQ. Firstly, to normalize for systematic technical errors every protein intensity detected in a particular slice was normalized by a factor calculated by comparison of protein intensities across all slices of the same number. For example, 702 proteins had intensity reported in all 6 peptide samples derived from slice 17. For all 702 proteins their intensity relative to the average intensity across all slice 17 samples was calculated, and the median of the 702 relative intensity values for a specific slice was used to normalize all protein intensities in that slice. This was repeated for all 21 slices to give slice-specific normalized

protein intensities. A weighted average method was used to derive an MW_{App} for every protein. For example, in the first NT siRNA replicate 60% of WDR18 (HUMAN WD repeat-containing protein 18) normalized protein intensity is detected in slice 16 (MW_{App} 41.9 kDa) and 40% in slice 17 (MWApp 35.4 kDa). Its MW_{App} would be reported as 39.3 kDa (0.6 × 41.9kDa + 0.4 × 35.4kDa). This was done independently for the two LC-MS/MS runs.

Data filtering and statistical analysis
For each protein detected in each NiNTA elution an MW_{App} was calculated. Only proteins with an MW_{App} reported in all 6 replicates were carried forward for further analysis. Owing to high variability in MW_{App} calculation for a small proportion of proteins MW_{App} %CV was calculated for both NT siRNA and SENP6 siRNA samples and for both LC-MS/MS runs. Only proteins for which all four %CV values were less than 30% were carried forward. This left 3441 proteins. For each LC-MS/MS run an average MW_{App} for the NT and SENP6 conditions was calculated for every protein. The difference MWAppSENP6-MWAppNT was used to determine how much a SUMO2-modified protein shifted in the gel upon SENP6 siRNA treatment. Statistical significance was calculated by student's t-test comparing the three MW_{App} values from NT condition with the three from SENP6 condition for each LC-MS/MS run. Charts were created using MW_{App}SENP6-MW_{App}NT and t test p values averaged across the two LC-MS/MS runs.

% Global protein intensity change
In post-translational modification proteomic experiments, considering only protein intensity ratios can overemphasise very small changes in absolute conjugation status and underemphasise large changes. For example, if a protein site occupancy increases from 1% to 6% (+5%) this gives a ratio of 6. However, an increase in occupancy from 10% to 30% only gives a ratio of 3 although a much greater proportion of the protein has become modified (+20%). To put SUMOylation changes between SENP6 depleted cells and controls into context of absolute SUMOylation we looked at the numerical difference (subtraction) in protein intensity between NT and SENP6 siRNA conditions (after normalization by all proteins intensity), and call this '% Global Protein Intensity change':

For each protein detected in each 6His-SUMO2 purification replicate, the proportion of all proteins intensity that it represented was calculated.

If the intensity of a protein p is i_p and the intensity of all detected proteins in the sample is i_{all} then;

$$\%Global\ Protein\ Intensity_p\ =\ i_p/i_{all} \times 100 \qquad \text{(Equation 1)}$$

If the % Global Protein Intensity of a protein p in the sample derived from cells treated with non-targeting siRNA is % $Global\ protein\ intensity_p^{NT}$ and the equivalent value derived from cells treated with SENP6siRNA is % $Global\ protein\ intensity_p^{SENP6}$, then the change to this value was calculated by;

$$\%\ Global\ Protein\ Intensity\ Change\ =\ \%\ Global\ Protein\ Intensity_{pSENP6}\ -\ \%\ Global\ Protein\ Intensity_{pNT} \qquad \text{(Equation 2)}$$

For example, Lamin-A protein intensity represented 0.331%, 0.249% and 0.308% of the total protein intensity in each of the SiNT replicates, but 0.666%, 0.656% and 0.745% of total protein intensity in each of the SiSENP6 treated replicates. The % Global Protein Intensity Change for lamin-A is the difference between the averages, which is therefore +0.393%. The value used in the study is the average of this value across the two mass spec runs.

A relatively large value for % Global Protein Intensity Change implies a relatively large absolute change in SUMOylation.

Immunofluorescence
Cells were plated on 13mm glass coverslips (VWR International) followed up by specific treatments. After treatment cells were carefully washed 3 times with PBS and fixed by incubating with 4% paraformaldehyde for 10min. Then cells were permeabilized with 0.2% Trition-X For 10min, washed 3 times with PBS and blocked with 5% BSA in PBS 0.1% Tween solution for 30min. Coverslips were washed 3 times with Wash Buffer (1% BSA in PBS 0.1% Tween) prior to incubation with primary antibody in Wash Buffer for 1h at room temperature. That was followed up with another washing sequence and incubation with secondary antibody for 45min and DAPI for 2min. Cells were again washed as before, dried and mounted on Superfrost Slides (VWR International). Immunofluorescence (IF) images were obtained using a Leica DM-IRB microscope equipped with a Hamamatsu CCD camera and 50x 0.3C-Plan lens or GE Deltavision Widefield using 60x oil lens. All images contain 10µm scale bars. Quantitation of cells with an altered nuclear structure and altered Lamin A distribution was done on a double blind basis. In randomly chosen immunofluorescence images of HeLa cells stained for Lamin A and DAPI, cells were judged to have either a normal nuclear structure with a clear nuclear rim staining for Lamin A or an abnormal nuclear structure displaying nuclear blebbing and an irregular pattern of Lamin A staining. As hiPSC did not display nuclear blebbing, cells were counted as normal if they displayed a brighter nuclear rim Lamin A signal with a lower signal inside the nucleus and cells that did not show a specific Lamin A signal at the nuclear envelope or undetectable nuclear Lamin A staining across the cell (probably absent due to out of focus light in wide field microscopy) were counted as abnormal. Microscope settings for imaging were exactly the same for all conditions. Experiments were carried out in triplicate with four fields of view being counted for each triplicate measurement. All 12 measurements are shown in the scatterplot.

In vitro transcription of PISM mRNAs

DNA template for mRNA transcription was obtained by PCR amplification of pCDNA5 FRT/TO containing PISMs with specific set of primers.

In vitro transcription, capping and polyadenylation of PISM mRNAs was performed using the mMESSAGE mMACHINE T7 ULTRA Transcription Kit (Thermo Fisher AM1345) and purified with the MEGAclear Transcription Clean-Up Kit (Thermo Fisher AM1908) according to the manufacturers' instructions. DNA templates were PCR amplified from the corresponding plasmids using the KOD Hot Start DNA Polymerase (Merck Millipore 71086) and purified by agarose gel electrophoresis using the QIAquick MinElute Gel Extraction Kit (QIAGEN 28604).

Alphafold model of a human lamin A dimer

The structure of lamin dimer was predicted using Alphafold2-multimer: https://colab.research.google.com/github/sokrypton/ColabFold/blob/main/AlphaFold2.ipynb#scrollTo=G4yBrceuFbf3.[58,59] The input sequence corresponded to human lamin isoform A (NCBI Reference Sequence: NP_733821.1). Unrelaxed top-ranked model based on AlphaFold pTM score was used.

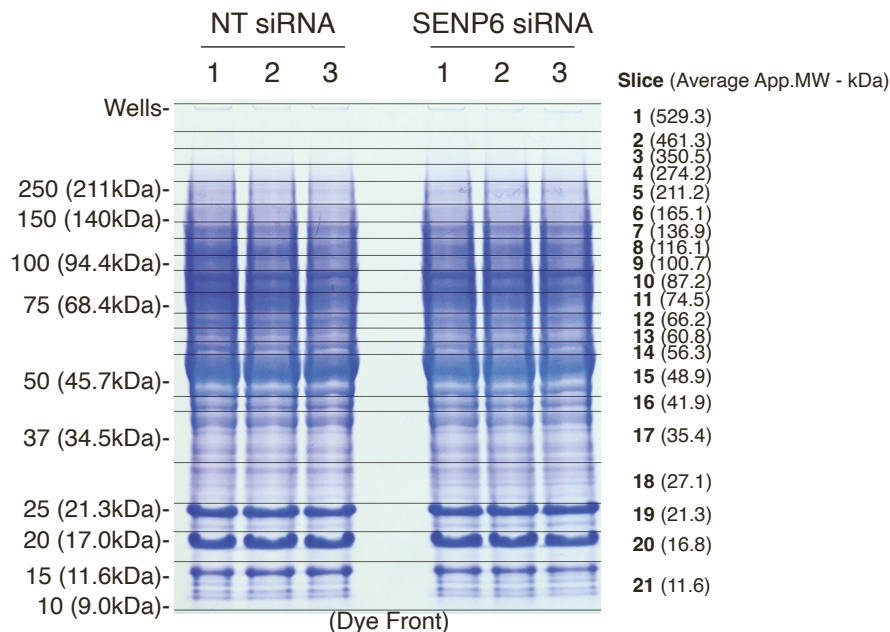## QUANTIFICATION AND STATISTICAL ANALYSIS

Specific details of statistical methods are described in figure legends and the Methods section. Manipulations and statistical analyses for mass spectrometry data were performed in Perseus and ExCel. Cell counting statistical analyses were conducted in PRISM. p values significance is defined as * <0.05; ** <0.01, *** <0.001, and **** <0.0001.

Supplemental information

SUMO protease SENP6 protects the nucleus

from hyperSUMOylation-induced

laminopathy-like alterations

Magda Liczmanska, Michael H. Tatham, Barbara Mojsa, Ania Eugui-Anta, Alejandro Rojas-Fernandez, Adel F.M. Ibrahim, and Ronald T. Hay

A

NiNTA purifications
(Coomassie staining)

Slice (Average App.MW - kDa)		
1 (529.3)
2 (461.3)
3 (350.5)
4 (274.2)
5 (211.2)
6 (165.1)
7 (136.9)
8 (116.1)
9 (100.7)
10 (87.2)
11 (74.5)
12 (66.2)
13 (60.8)
14 (56.3)
15 (48.9)
16 (41.9)
17 (35.4)
18 (27.1)
19 (21.3)
20 (16.8)
21 (11.6)

B

Distance from well (Arb)	Retention factor	Marker App.MW (Da)	Log10 Marker App.MW
2.55	0.169	211000	5.324
3.45	0.228	139700	5.145
4.83	0.319	94400	4.975
6.23	0.412	68400	4.835
8.52	0.563	45700	4.660
10.08	0.666	34500	4.538
12.36	0.817	21300	4.328
13.19	0.872	17000	4.230
14.31	0.946	11600	4.064
15.13	1.000	9000	3.954

$y = -3.122x^3 + 5.4656x^2 - 4.2968x + 5.8946$
$R^2 = 0.9995$
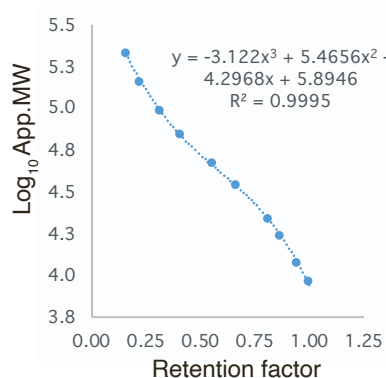
C

Slice number	Lower cut distance from well (Arb)	Lower cut Retention factor	Lower cut Log10 App.MW*	Lower cut App.MW	Slice number	Average App.MW of slice
1	0.64	0.0420	5.72	529251	1	529251§
2	1.17	0.0770	5.59	393305	2	461278
3	1.65	0.1087	5.49	307630	3	350468
4	2.17	0.1434	5.38	240744	4	274187
5	2.85	0.1880	5.26	181609	5	211177
6	3.39	0.2237	5.17	148560	6	165084
7	3.90	0.2574	5.10	125144	7	136852
8	4.41	0.2915	5.03	106961	8	116052
9	4.86	0.3209	4.98	94503	9	100732
10	5.53	0.3654	4.90	79800	10	87152
11	6.17	0.4075	4.84	69189	11	74495
12	6.61	0.4365	4.80	63198	12	66194
13	7.02	0.4640	4.77	58311	13	60755
14	7.41	0.4898	4.73	54256	14	56284
15	8.70	0.5747	4.64	43434	15	48845
16	9.14	0.6041	4.61	40293	16	41864
17	10.71	0.7075	4.48	30533	17	35413
18	11.94	0.7892	4.37	23616	18	27075
19	12.81	0.8463	4.28	19072	19	21344
20	13.71	0.9058	4.17	14679	20	16875
21	15.19	1.0036	3.93	8539	21	11609

Figure S1. Using gel retention factor to determine apparent MW for proteins. Related to Figure 1.
A. Coomassie-stained gel of triplicate NiNTA purifications from 6His-SUMO2 cells treated either with non-targeting (NT) siRNA or SENP6 siRNA. Positions of molecular weight markers are indicated with their apparent MW in this gel system shown in brackets. The positions of 21 gel slices made for the analysis are indicated (right) along with the designated average apparent MW of the slice (parentheses). B. Table (left) showing the calculated retention factor values for each of the molecular weight markers from A. B (right) The relationship between retention factor and log$_{10}$ App.MW for the MW markers shown in A. C. Table of calculations for average App.MW for each of the 21 slices shown in A. *Calculated using the equation in B (right). §For slice 1 the AppMW value of the lower cut alone was used.
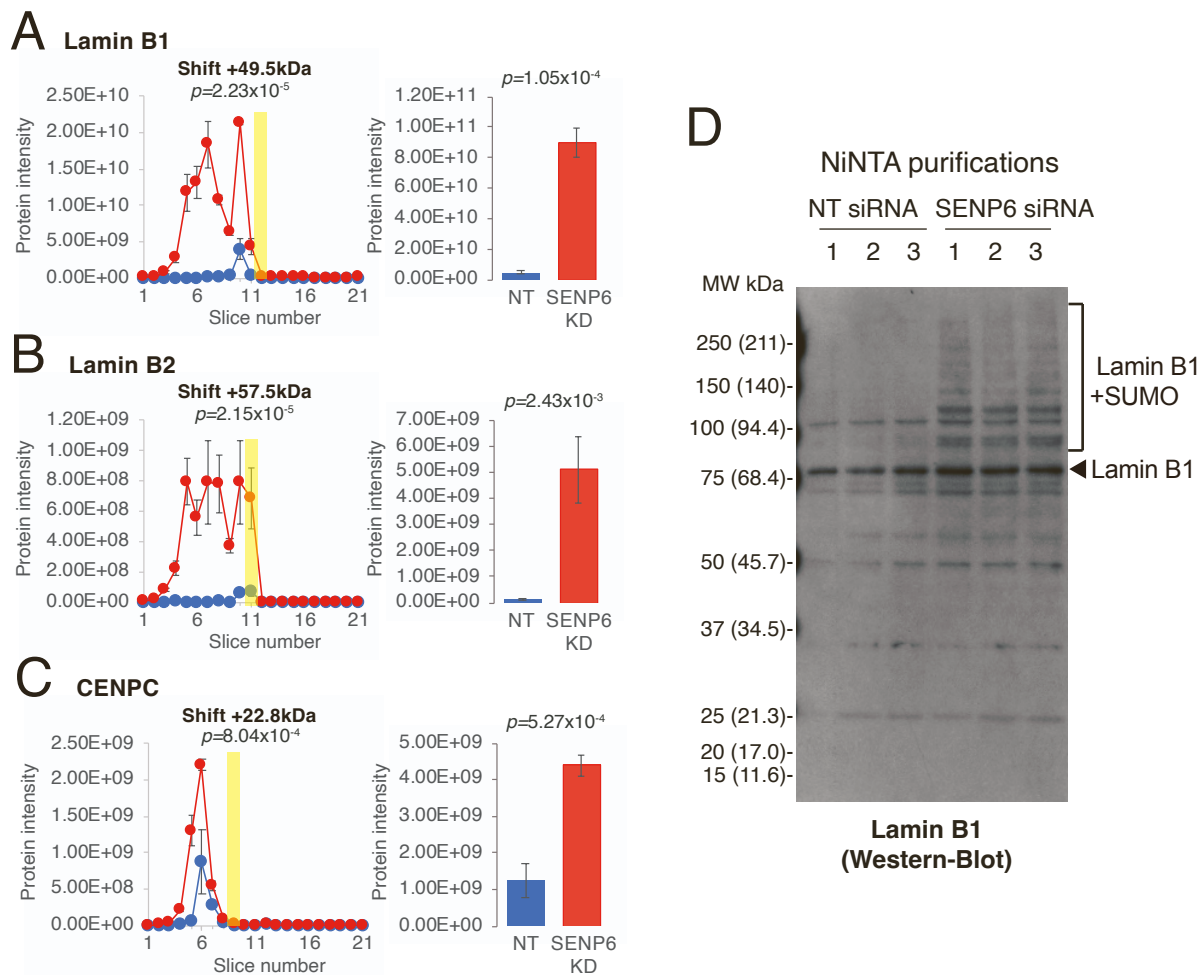
Figure S2. Selected examples of proteins that show reduced electrophoretic mobility in SUMO2 enrichments upon SENP6 knock-down. Related to figure 2.
A-C. Protein intensity per slice profile plot (left) and total protein intensity (right) with SD values shown as error bars for the indicated proteins. Points represent the average of the triplicate intensity data summed across the two MS runs. p values are calculated by unpaired two-tailed student's t-tests for both MW change and overall protein intensity change. Yellow bar indicates the gel slice predicted to contain unmodified protein according to amino-acid sequence alone. D. Lamin B1 Western Blot of NiNTA purifications from 6His-SUMO2 cells after the indicated siRNA treatment. Markers show MW in kDa with apparent MW in this gel system shown in brackets.
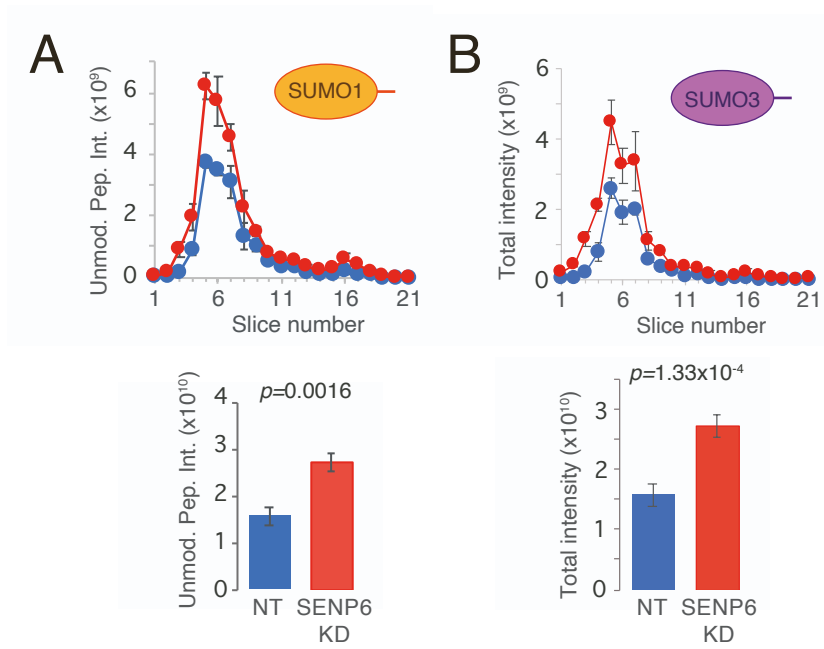
Figure S3. Increase in SUMO1 and SUMO3 in 6His-SUMO2 purifications upon SENP6 depletion
A&B. Total unique peptide intensity for SUMO1 and SUMO3 shown either separated by slice (upper) or as a sum total (lower). Only peptides unique to SUMO1 or SUMO3 were used to calculate protein intensity. Peptides from SUMO3 in common with SUMO2 were omitted. Points represent the average of the triplicate intensity data summed across the two MS runs. SD values shown as error bars. Student's t-test p is indicated.
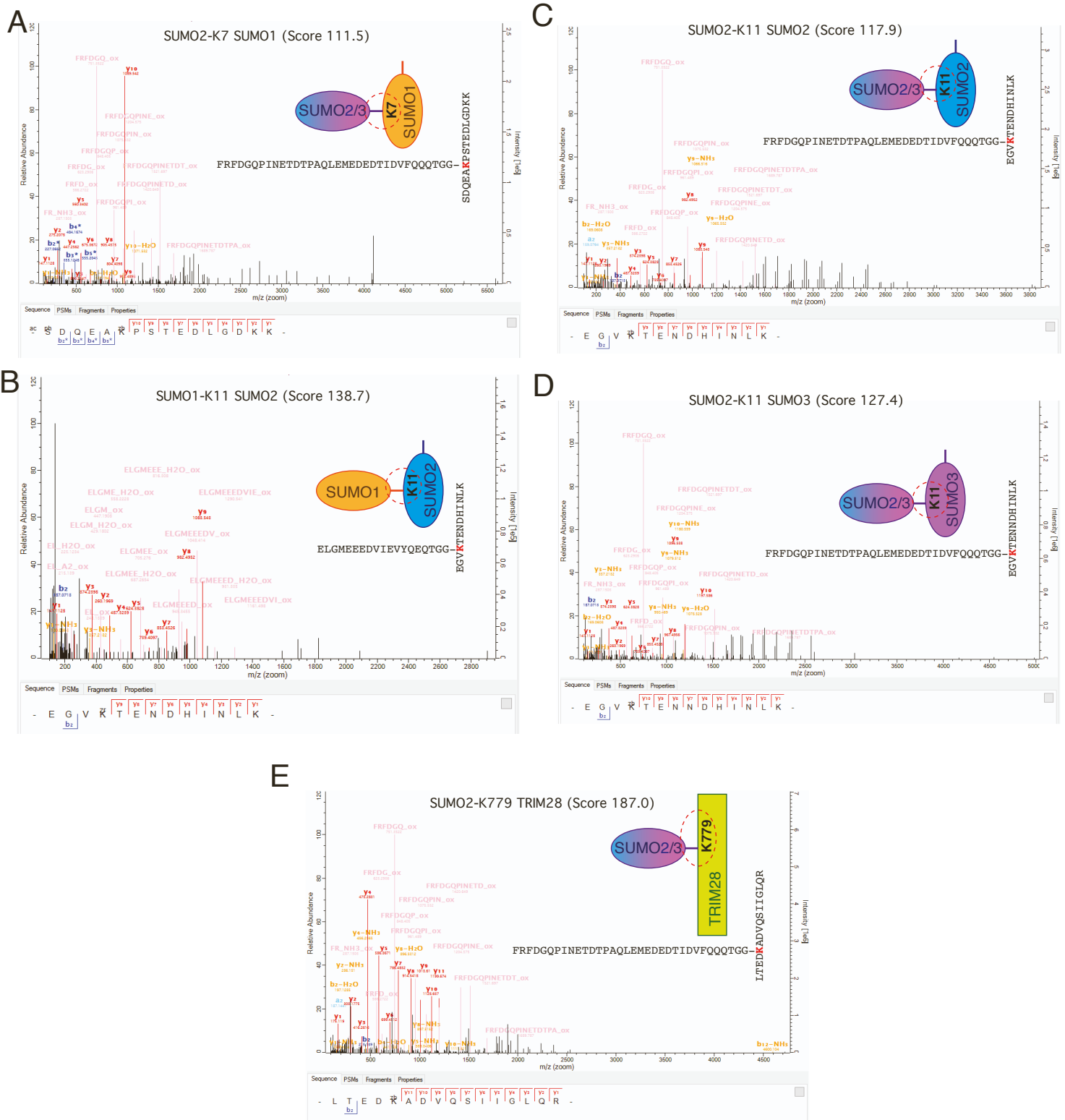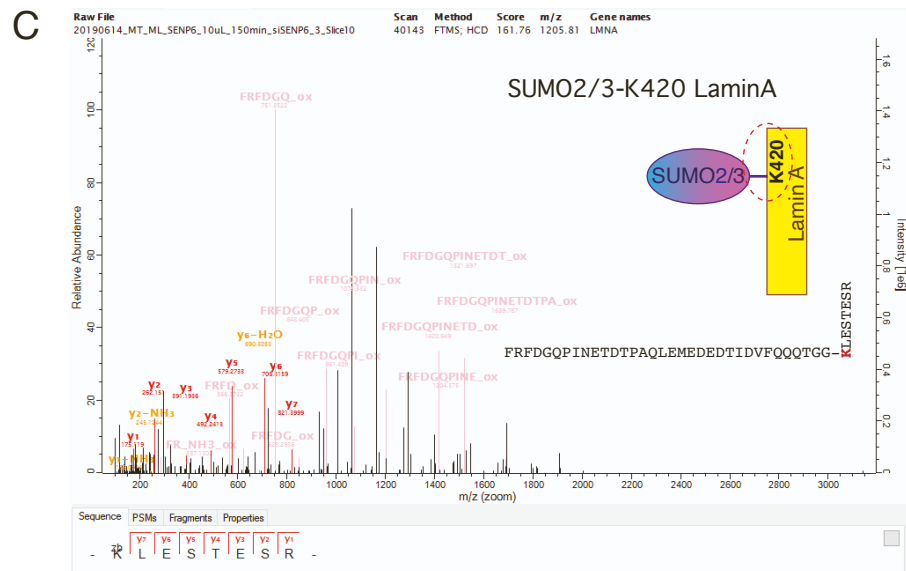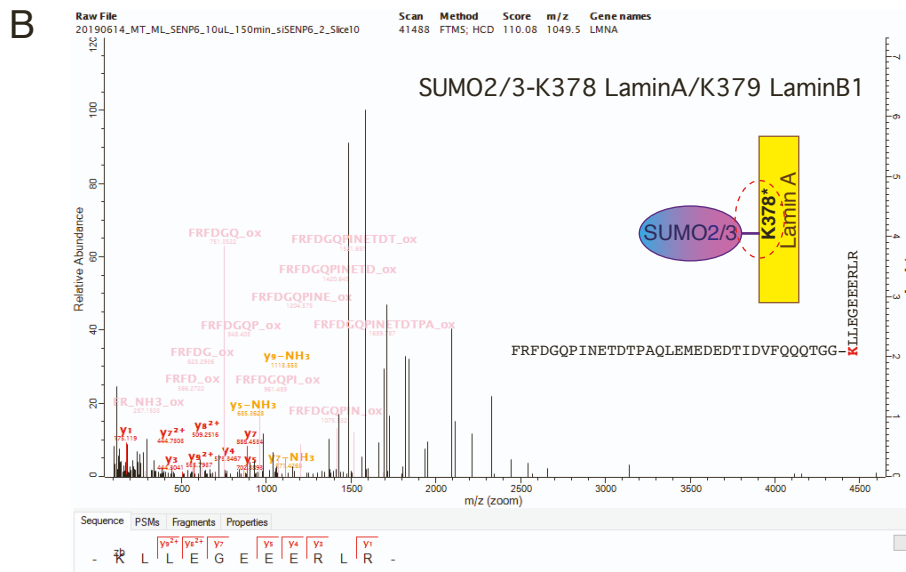
Figure S4. MS/MS spectra for SUMO-SUMO and SUMO-TRIM28 branched peptides. Related to figure 3.

A-E. MaxQuant MS/MS spectra annotations for the SUMO2-LaminA (A-D) and SUMO2-TRIM28 (E) peptides used for the quantification shown in Figure 3E-I. b series ions derived from the C-terminal (donor) SUMO portion of the branched peptide are shown in pink. Unannotated high intensity peaks in the high m/z region are y-series derived from the fragmentation of the donor SUMO sequence and are not annotated automatically by MaxQuant. Acceptor lysines are indicated by K with "zp" (SUMO1) or "zb" (SUMO2/3) above.
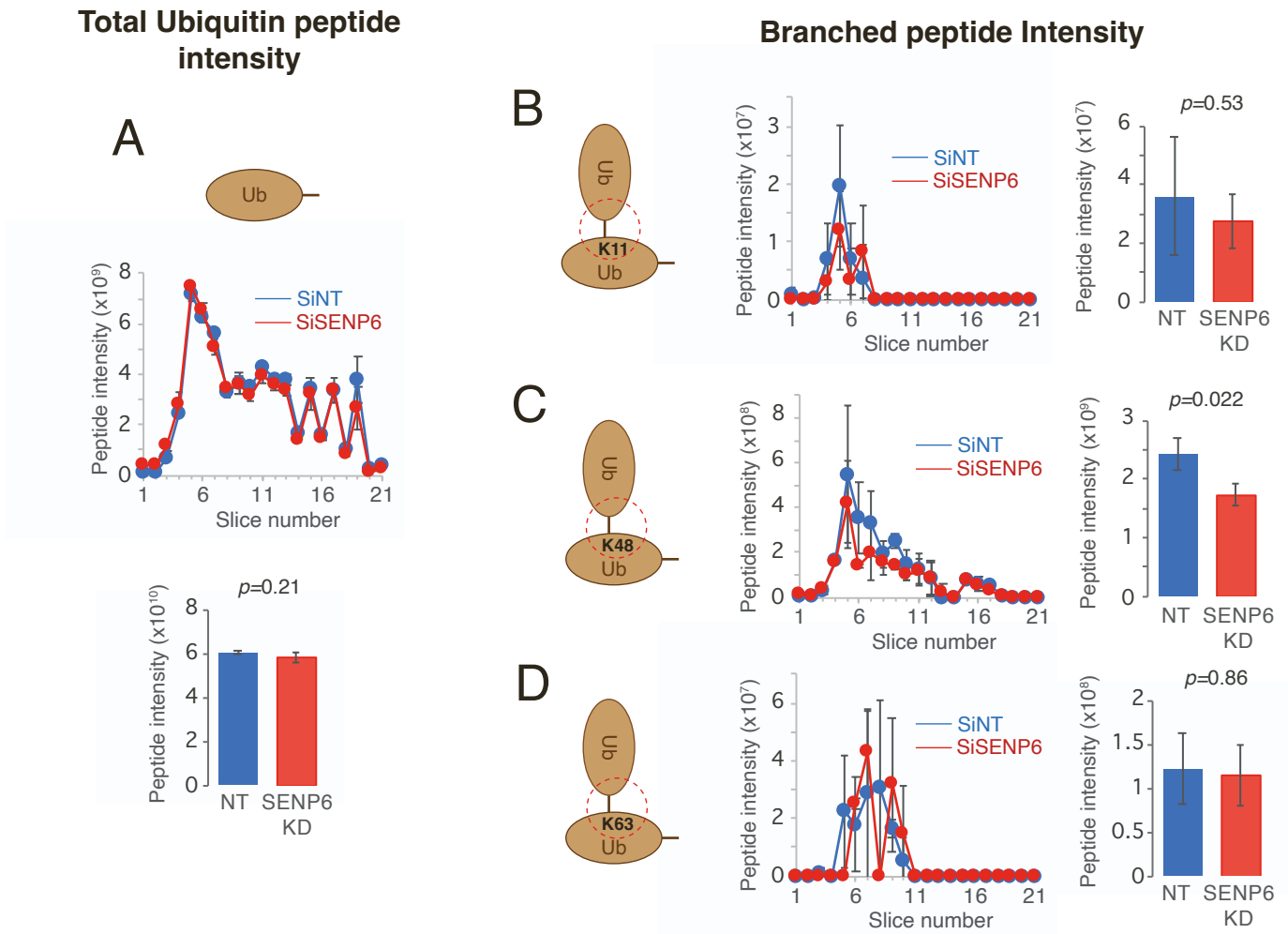
Figure S5. Ubiquitin-Ubiquitin branched peptides associated with SUMO2 are not increased in abundance upon SENP6 depletion. Related to figure 3.

A. Peptide intensity profile plot and total peptide intensity data for all ubiquitin peptides (except Ub-Ub branches). Points represent the average of the triplicate intensity data summed across the two MS runs. SD values shown as error bars. Student's t-test p is indicated. B-D. Equivalent plots as in A for branched peptides indicative of Ubiquitin-Ubiquitin conjugates depicted in the schematics (left).
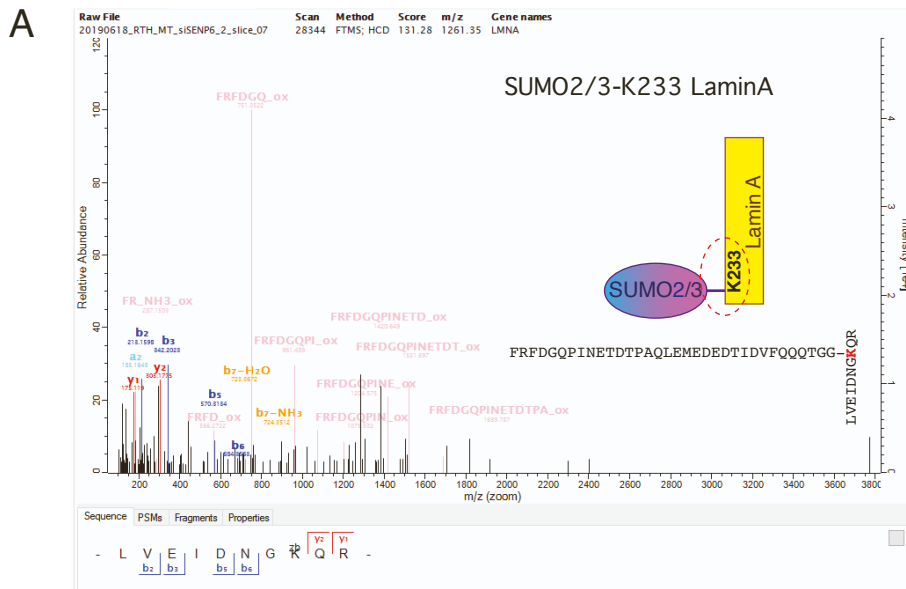
Figure S6. MS/MS spectra for SUMO2/3-Lamin A branched peptides. Related to figure 3.
A-C. MaxQuant MS/MS spectra annotations for the SUMO2-LaminA peptides used for the quantifi-
cation shown in Figure 3 A-D. b series ions derived from the SUMO2 portion of the branched
peptide are shown in pink. Unannotated high intesnity peaks in the high m/z region are y-series
derived from the fragmentation of the SUMO2 portion attached to the whole LaminA peptide and
are not annotated automatically by MaxQuant. Acceptor lysines are indicated by K with "zb" above.
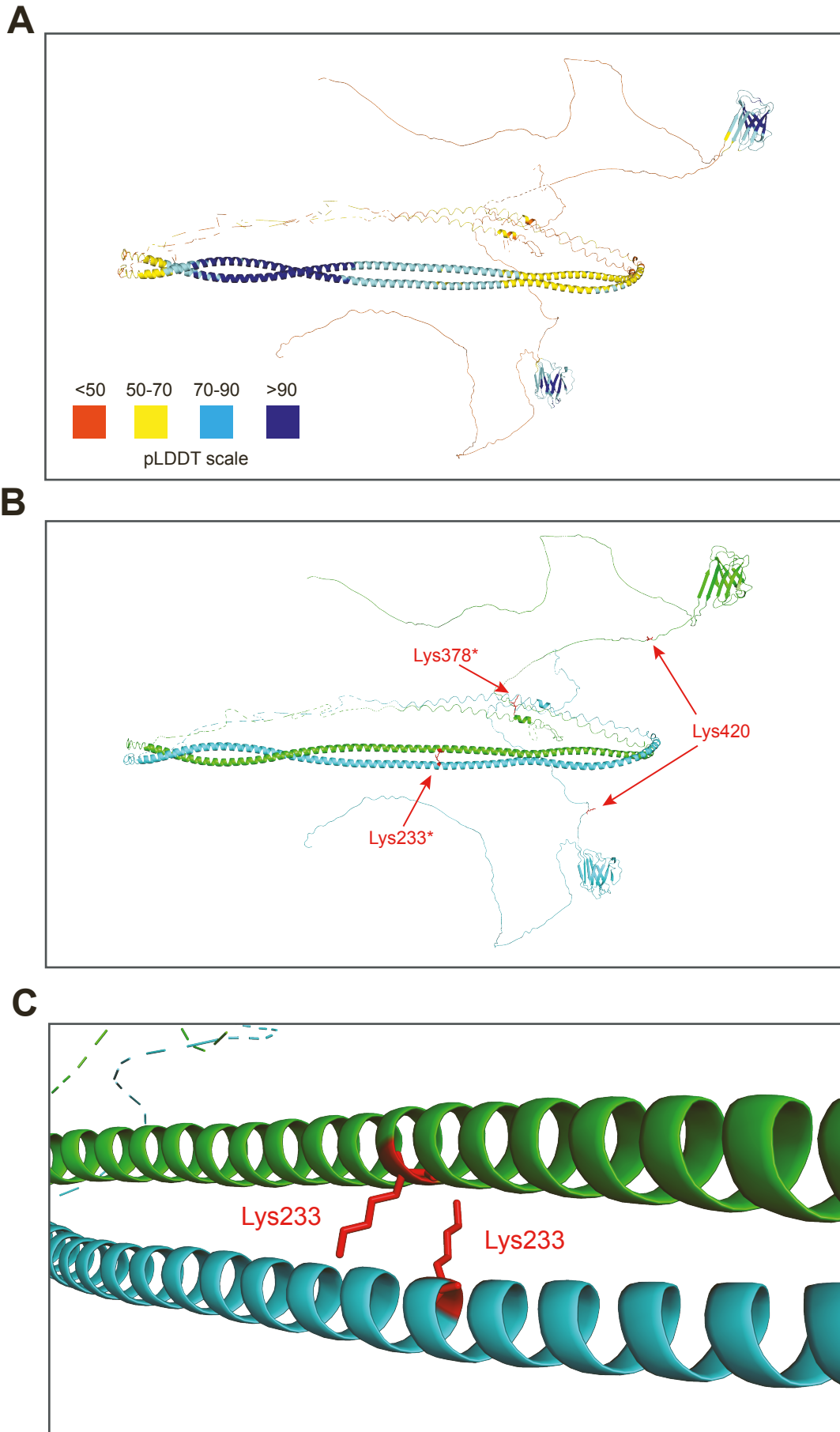
Figure S7. Alphafold model of a Lamin A dimer. Related to figure 4.
A+B. Full view of the Alphafold model of a human LaminA dimer coloured by pLDDT score (A) or by monomer: green and cyan chains (B) with SUMO attachment sites labelled. *Residues from both monomers are in close proximity. C. Zoom view of Lysine 233 at the helical dimer interface. SUMO modified lysines are shown in stick format in red and labelled.
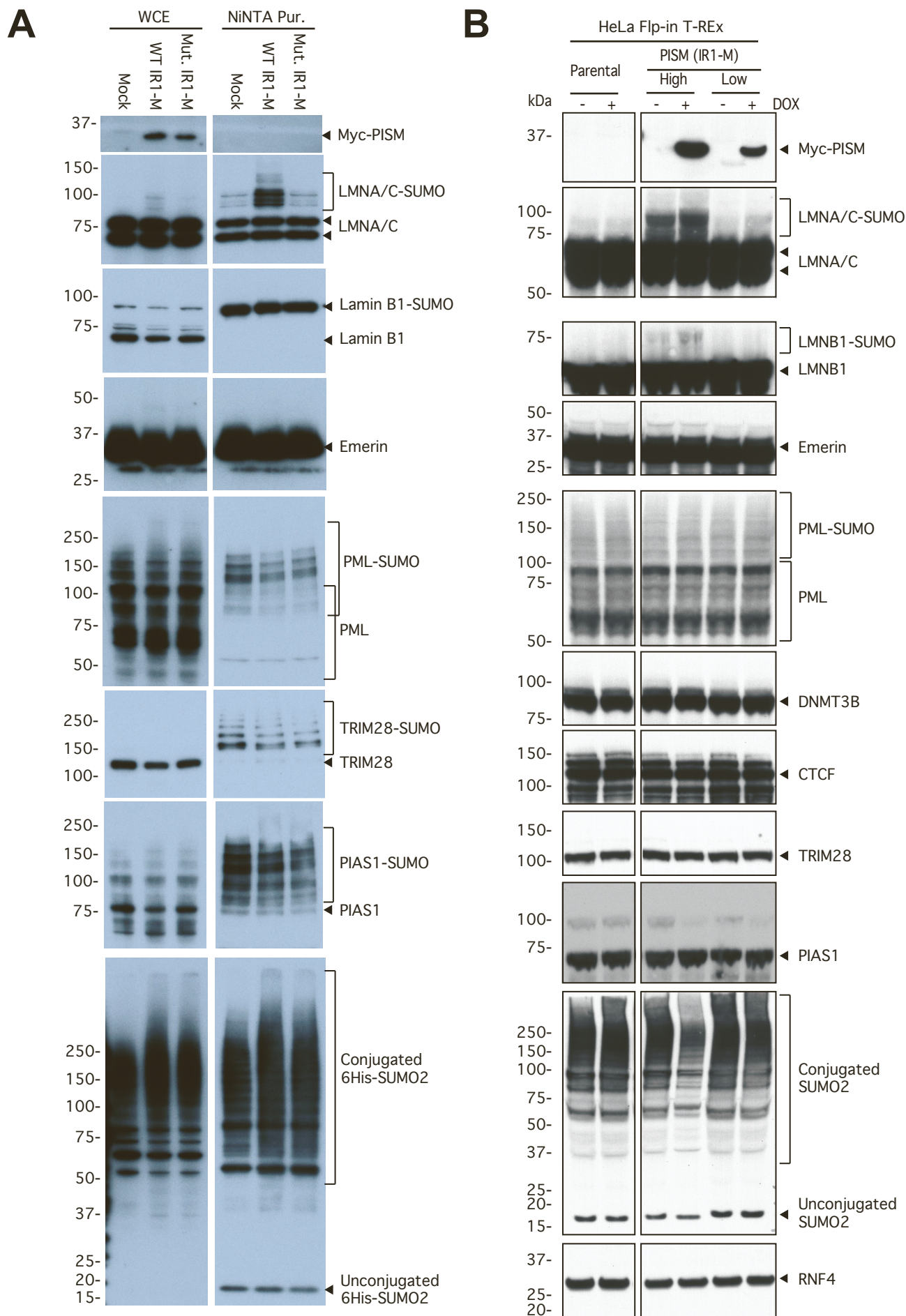
Figure S8. Specificity of the Lamin A PISM construct. Related to Figure 6.
A. 6His-SUMO2 HeLa cells transfected with mRNA for the WT IR1-M or mutant IR1-M PISM construct, or mock transfected. Western blots for the indicated proteins were performed on Crude whole cell extracts (WCE) or Nickel NTA purifications (NiNTA Pur.). B. HeLa Flp-In T-REx cells containing the indicated PISM constructs inducible by DOX were either DOX treated or not and the indicated proteins detected by Western blot from crude whole cell extracts. Data derived from single blots cropped to remove irrelevant lanes (see Source data DOI: 10.17632/bsxmfv7stg.1)
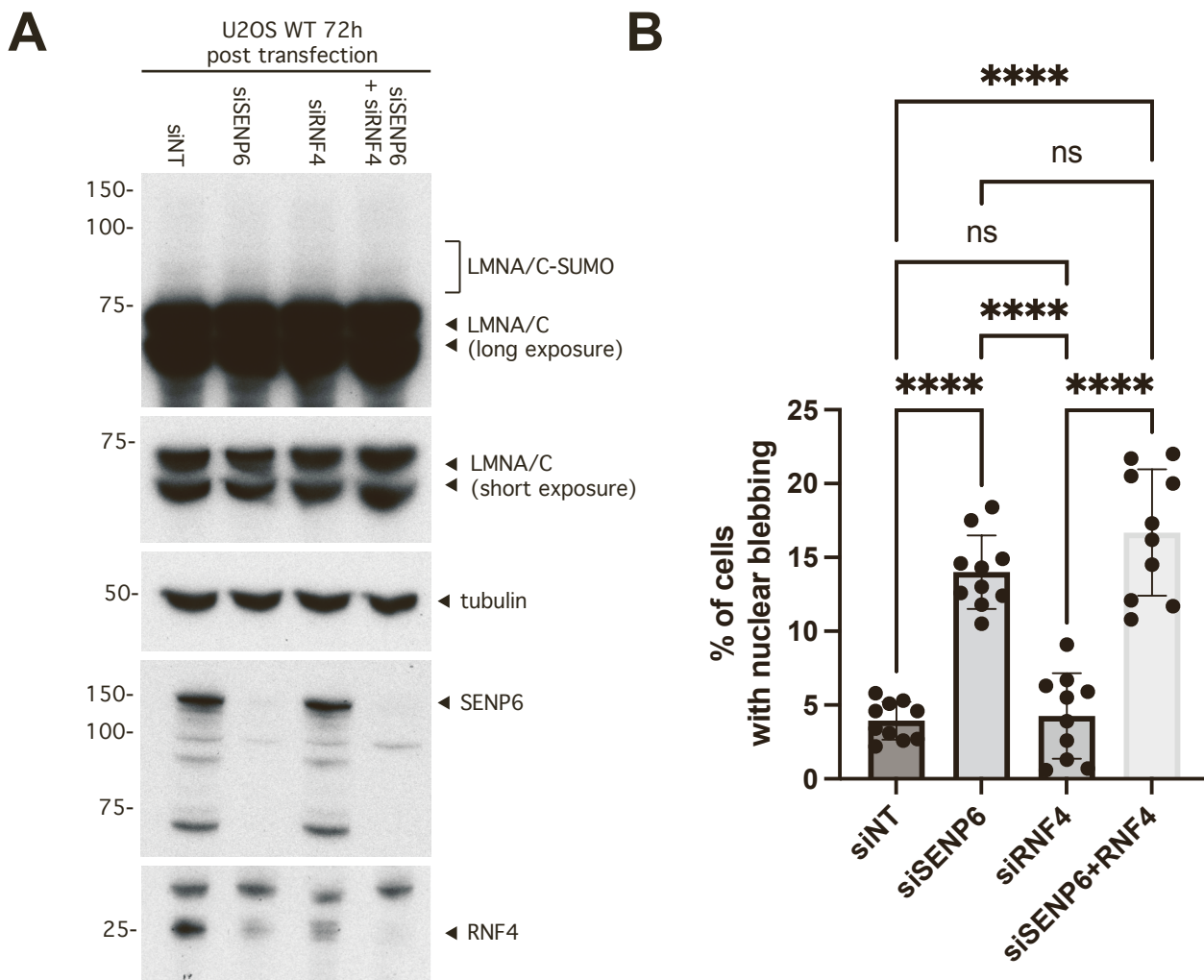
Figure S9. Ruling out the involvement of RNF4 in the SENP6-mediated phenotype. Related to figure 4.

A. Crude whole cell extracts were prepared from WT U2OS cells transfected with siRNAs against SENP6 and/or RNF4, or non-targeting (NT) siRNA 72h after tranefctions. Whole cell extracts were analysed by Western blot for the indicated proteins. B. Corresponding IF samples were fixed and stained using an anti-LMNA/C antibody, imaged and further analysed for the presence of nuclear blebbing pheneotype. Data was plotted as mean +/- SD (each point represents a single image containing between 50 and 150 cells) and statistical analysis was performed using one-way ANOVA (Tukey's multiple comparison test) in GraphPad PRISM. 10 fields were surveyed per condition.

Table S1. - Oligonucleotides used in this study.

Oligo name	Sequence (5'-3')
IR-M elimination of IR2 Forward primer	ACAGCAGATAATGAGAAAGAATGTATTTAGGCGGCCGCTCGAGTCTAG
IR-M elimination IR2 Reverse primer	TAAACGGGCCCTCTAGACTCGAGCGGCCGCCTAAATACATTCTTTCTC
RanBP2 cat.dom mutations Forward	GAGCAGAAAGCCCTTGCAACCAAAGCGAAAGCGGCTCCAACTGCCGCCTCCTACAAGAAT
RanBP2 cat.dom mutations REV	AACATAATCTGGTCTATTCTTGTAGGAGGCGGCAGTTGGAGCCGCTTTCGCTTTGGTTGC
E3_5 Forward mRNA	TAATACGACTCACTATAGGGAGAGCCACCATGGAGCAGAAGCTCATAAG
LaA_7 Forward mRNA	TAATACGACTCACTATAGGGAGAGCCACCATGGAGCAAAAGCTCATTTCC
DARPin Forward	AAAAAAAAGCTTGCCACCATGG
E5_3 Reverse	AAAAAAGCTAGCCTGCAAAATCTCT
LaA_7 Reverse	AAAAAAGCTAGCGTTGAGTTTTGC